

## End-To-End Capacities of Hybrid Quantum Networks

Cillian Harney<sup>1</sup>,\* Alasdair I. Fletcher<sup>1</sup>, and Stefano Pirandola

*Department of Computer Science, University of York, York YO10 5GH, United Kingdom*

 (Received 13 September 2021; revised 27 January 2022; accepted 15 April 2022; published 7 July 2022)

Future quantum networks will be hybrid structures, constructed from complex architectures of quantum repeaters interconnected by quantum channels that describe a variety of physical domains; predominantly optical-fiber and free-space links. In this hybrid setting, the interplay between the channel quality within network substructures must be carefully considered, and is pivotal for ensuring high-rate end-to-end quantum communication. In this work, we combine recent advances in the theory of point-to-point free-space channel capacities and end-to-end quantum network capacities in order to develop critical tools for the study of hybrid, free-space quantum networks. We present a general formalism for studying the capacities of arbitrary, hybrid quantum networks, before specifying to the regime of atmospheric and space-based quantum channels. We then introduce a class of modular quantum network architectures, which offer a realistic and readily analyzable framework for hybrid quantum networks. By considering a physically motivated, highly connected modular structure we are able to idealize network performance and derive channel conditions for which optimal performance is guaranteed. This allows us to reveal vital properties for which distance-independent rates are achieved, so that the end-to-end capacity has no dependence on the physical separation between users. Our analytical method elucidates key infrastructure demands for a future satellite-based global quantum internet, and for hybrid wired and wireless metropolitan quantum networks.

DOI: [10.1103/PhysRevApplied.18.014012](https://doi.org/10.1103/PhysRevApplied.18.014012)

### I. INTRODUCTION

The current internet is a vast classical network, designed to facilitate global communication and distributed information processing [1–4]. The inherent robustness of classical information allows for hybrid, flexible network architectures, which operate in both optical fiber and free space, befitting an environment and mode of application. A future quantum internet will aim to play an analogous role for quantum-information technologies [5–8], but the inherent fragility of quantum information makes achieving high rates over long distances much more challenging. In pursuit of this goal, theoretical and experimental progress in the study of hybrid quantum networks is fundamental and necessary.

The ultimate limits of fiber networks are well understood. By means of the Pirandola-Laurenza-Ottaviani-Banchi (PLOB) bound, it is known that the capacity of a fiber link decays exponentially with respect to the link length with a precise law [9,10]. The PLOB bound has been used to understand the end-to-end network capacities of fiber-based quantum architectures [11], to assess the limits of realistic, random network structures [12,13] and idealized, highly connected, analytical architectures [14]. These investigations have provided essential insight

and motivation for the construction of high-performance quantum networks, elucidating key physical properties and network characteristics. Chiefly, to develop a high-performance, fiber-based quantum network one must carefully consider not only connectivity, but nodal density and maximum link length; leading to high resource demands for large-scale designs.

However, quantum networks will not be limited to just optical fiber but will collaborate with free-space methods of communication. On the ground, the flexibility of free-space links are obviously more suitable for mobile quantum devices and short-range connections. Meanwhile, the ability to establish ground-to-satellite and intersatellite free-space connections offers remarkable short cuts for global quantum communications [15–21]. Such connections bypass many decibels of loss that would be otherwise experienced on the ground, and utilize the dynamic nature of satellites to achieve high rates over global distances.

Determining the ultimate limits of free-space quantum channels is difficult, requiring tools from quantum-information theory [22–24], optics [25–27], and turbulence theory [28–31]. Recent advancements have placed tight upper bounds on the quantum capacities of point-to-point free-space channels, using a modified PLOB bound that accounts for atmospheric fading processes [32,33]. With these results in hand, we have the ingredients to go beyond the point-to-point scenario and quantitatively study the

\*cth528@york.ac.uk

ultimate limits of communications in free-space quantum networks.

In this work, we combine results from Refs. [11,32,33] in order to place bounds on the end-to-end capacities of generally hybrid quantum networks. In particular, we put forward a formalism for studying the capacities of quantum networks whose channels are described by free space, fiber, or any medium that can be generalized as a fading channel. This treatment is then specified to fading processes that are experienced by optical transmissions through the atmosphere, or in space.

Furthermore, we introduce a framework to investigate the ultimate limits of hybrid, modular quantum networks. We focus on a modular network design, which consists of disjoint subnetworks (or communities) connected to a large-scale backbone network used to mediate intercommunity quantum communication. This provides the tools to investigate highly relevant quantum-network models, such as globally distant fiber subnetworks connected to a satellite backbone network, offering insight into the resource requirements of a satellite-based quantum internet; and wireless, free-space subnetworks on the ground interconnected via a fiber backbone, presenting a useful model for studying hybrid metropolitan networks.

Extending the techniques of Ref. [14] we employ ideally connected structures within different parts of the modular network. In doing so, we are able to derive simple, yet powerful analytical constraints, which promise distance-independent rates for modular quantum architectures, and thus optimal performance. These results provide valuable insight into the ultimate limits of hybrid networks, can help to motivate future quantum-network designs and provide a valuable platform upon which to further develop realistic free-space quantum networks.

### A. Paper structure

This paper is structured as follows: In Sec. II we provide a comprehensive review of quantum networks, point-to-point capacities of general fading channels and the end-to-end network capacities of quantum networks generally composed of fading channels. We then specify this review to optical free-space quantum communications, summarizing recent progress in the determination of ultimate limits for a number of key settings. In Sec. III we formalize a network architecture for the study of hybrid, modular quantum networks. We further specify an idealized network architecture, which allows us to establish properties that guarantee optimal end-to-end performance and distance independence. Finally, Sec. IV applies the machinery from the previous sections to investigate the optimal performance of hybrid quantum architectures. In particular, we establish network constraints for communication between remote fiber-based subnetworks connected to a satellite backbone, and for ground-based free-space

subnetworks connected to a fiber backbone. Concluding remarks and future investigative paths are then discussed.

## II. PRELIMINARIES

### A. Quantum networks

An arbitrary quantum network can be described as a finite, undirected graph  $\mathcal{N} = (P, E)$  where  $P$  is the set of all network nodes (points and vertices) on the graph, and  $E$  is the set of all edges within the network. Each node  $\mathbf{x} \in P$  represents a local register of quantum systems, which can be exchanged with connected neighbors. Meanwhile each edge in the network is denoted by the unordered pair  $(\mathbf{x}, \mathbf{y}) \in E$ , and is used to represent a quantum channel  $\mathcal{E}_{\mathbf{x}\mathbf{y}}$  through which users can exchange quantum systems. Two nodes  $\mathbf{x}$  and  $\mathbf{y}$  are connected if the edge  $(\mathbf{x}, \mathbf{y})$  exists within  $E$ .

It is worthwhile to note that the physical orientation of each channel  $\mathcal{E}_{\mathbf{x}\mathbf{y}}$  in the network can be a forwards or backwards and need not be specified. Under the assistance of two-way classical communications (CCs), the optimal transmission of quantum information is connected with optimal entanglement distribution. It does not depend on the physical direction of system exchange but the local operations (LOs) that are applied at each point, and thus the direction of teleportation. This refers to the *logical direction* of quantum communication. If an undirected edge represents a physically asymmetric channel (i.e.,  $\mathcal{E}_{\mathbf{x}\mathbf{y}} \neq \mathcal{E}_{\mathbf{y}\mathbf{x}}$ ) then the users can always enable a teleportation protocol that uses the most efficient physically directed channel. Hence, the logical flow of quantum information can always be made independent of the physical flow of quantum systems.

Consider two end users Alice and Bob, who reside at remote nodes within the quantum network,  $\alpha$  and  $\beta$ , respectively. An end-to-end communication protocol between Alice and Bob can be most broadly captured by a general adaptive protocol. Alice and Bob propagate the exchange of quantum systems between nodes throughout the network in accordance with an overarching protocol in order to establish some global, target quantum state. This may involve point-to-point, or point-to-multipoint exchanges dependent on the nature of the protocol. Quantum interactions between any two nodes is alternated with adaptive network-wide LOCCs, allowing for consistent optimization of the network protocol. Communication is complete when the target state is eventually established between the end users after a number of uses of the network.

The optimal performance over any such network protocol is captured via the generic two-way assisted network capacity  $\mathcal{C}(\mathcal{N})$ , which describes the ultimate rate with which a desired target state can be established. If the target is a private state, this refers to the network secret-key capacity  $K(\mathcal{N})$  measured in secret bits per network use. If

it is a maximally entangled state then this becomes the network entanglement distribution capacity  $E(\mathcal{N})$  measured in entanglement bits (ebits) per network use.

Note that we consider a general information-theoretic definition of a quantum repeater as a middle third party helping the quantum communication between a sender and a receiver (therefore not connected by a direct link). In practice, there are many possible physical realizations, e.g., see Refs. [34–36] among others.

### 1. Network routing

Thanks to the interconnectivity of quantum networks, there is no unique path that network interactions must follow in order to establish end-to-end quantum communication. However, there exist two fundamental classes of routing strategy under which all protocols can be described: *single-path* or *multipath* routing.

Single-path routing is the simplest network communication method, which utilizes point-to-point communications in a sequential manner. Quantum systems are exchanged from node to node followed by LOCC operations after each transmission until eventually communication has been established between the end users. One may define a single-path network capacity  $\mathcal{C}^s(\mathcal{N})$ , which describes the optimal performance obtained via a sequential end-to-end strategy. A repeater chain forms a particular instance of quantum network under single-path routing where there exists only one unique end-to-end route.

A more powerful strategy is multipath routing, which properly exploits the multitude of possible end-to-end routes available in a quantum network. A user may exchange an initially multipartite quantum state with a number of neighboring receiver nodes, who may each then perform their own point-to-multipoint exchanges along their unused edges. Again, every exchange of quantum systems can be interleaved with adaptive network LOCCs, and this process continues until multipoint interactions are carried out with the end users. A multipath routing strategy in which all channels in the network are used precisely once per end-to-end transmission is known as a *flooding protocol*. This is achieved via nonoverlapping point-to-multipoint transmissions at each network node, such that receiving nodes choose only to transmit along unused edges for subsequent connections. Therefore, there exists a multipath network capacity (or flooding capacity)  $\mathcal{C}^m(\mathcal{N})$ , which describes the optimal network performance out of all possible strategies (single or multipath).

### B. Quantum networking over fading channels

The effect of *fading* refers to the temporal variation of transmissivity along a bosonic lossy channel. The transmissivity along a fading channel is not fixed, but instead follows a probability distribution described by the dynamics of the environment. For example, the propagation of

bosonic modes through low-altitude free space instigates a fading channel thanks to chaotic processes in the atmosphere. The impact of fading on a communication channel is described via its *speed*, i.e., the ability for a receiver to resolve the dynamics of the transmissivity fluctuations. Slow fading implies that the users can resolve the fading dynamics and accurately perform channel estimation because either the fading process is weak or the users possess sufficiently fast detectors. On the other hand, fast fading refers to the situation where the users cannot reconcile the dynamics of the channel and can estimate only the statistical distribution of the channel transmissivity [37,38]. It is clear that fast fading poses a more formidable task for communicators.

More precisely, a bosonic lossy fading channel is defined as an ensemble of lossy channels in accordance with some probability density function  $F(\tau)$ , which describes the instantaneous transmissivity along the channel. We denote a lossy fading channel as the ensemble

$$\mathcal{E}_F(\eta) := \{F(\tau); \mathcal{E}_\tau\}, \quad (1)$$

where  $\mathcal{E}_\tau$  is a lossy channel with fixed, instantaneous transmissivity  $\tau \in [0, \eta]$  and  $\eta$  is the maximum transmissivity that is attainable along the channel.

#### 1. Capacities of fading channels

The absolute maximum rate that two parties can transmit qubits, establish secret keys, or distribute entanglement over bosonic lossy channels is known exactly via the PLOB bound [10]. This states that generic two-way assisted capacity of a quantum channel is precisely

$$\mathcal{C}(\mathcal{E}_\eta) = \mathcal{B}(\eta) := -\log_2(1 - \eta) \quad (2)$$

measured in bits per channel use, and where we introduce  $\mathcal{B}(\eta)$  as the capacity function for stable lossy channels. While this assumes a fixed transmissivity  $\eta$ , the PLOB bound can be readily employed to study fading channels [10,39]. Thanks to convexity properties of the relative entropy of entanglement (REE) over ensembles of channels, the capacity of a lossy fading channel can be bounded according to

$$\mathcal{C}[\mathcal{E}_F(\eta)] \leq \mathcal{B}_F(\eta) := \int_0^\eta d\tau F(\tau) \mathcal{B}(\tau), \quad (3)$$

where we define  $\mathcal{B}_F(\eta)$  as the capacity function for lossy fading channels. This can be interpreted as a generalization of Eq. (2), modified to include potential fading processes. Indeed, it is simple to retrieve the standard bound  $-\log_2(1 - \eta)$  for fixed lossy channels by considering a trivial probability distribution where only one transmissivity value is possible,  $\eta$ . Hence, this format is

conveniently general and allows one to describe any lossy bosonic channel (with or without fading).

More generally, lossy channels will also be exposed to thermal noise, resulting in a thermal-loss channel  $\mathcal{E}_{\tau, \bar{n}}$ . This channel equates to mixing an input mode with a thermal mode of mean photon number  $\bar{n}_e = \bar{n}/(1 - \tau)$  on a beam splitter of transmissivity  $\tau$ , effectively adding  $\bar{n}$  photons to the signal mode. The capacity of thermal-loss channels is not known exactly, but upper bounds have been derived through the techniques developed for the PLOB bound. For a fixed thermal-loss channel  $\mathcal{E}_{\tau, \bar{n}}$  the capacity can be upper bounded via [10]

$$\mathcal{C}(\mathcal{E}_{\tau, \bar{n}}) \leq \mathcal{L}(\tau, \bar{n}) := -\log_2(\tau^{\bar{n}_e}(1 - \tau)) - h(\bar{n}_e), \quad (4)$$

where  $h(x) := (x + 1) \log_2(x + 1) - x \log_2(x)$ . Otherwise  $\mathcal{L}(\tau, \bar{n}) = 0$  when  $\tau < \bar{n}$ , meaning that there exists a minimum transmissivity at which communication can be reliably secured.

Analogous to the pure-loss setting, a thermal-lossy fading channel can be described by the ensemble

$$\mathcal{E}_F(\eta, \bar{n}) := \{F(\tau, \bar{n}); \mathcal{E}_{\tau, \bar{n}}\}, \quad (5)$$

where it is possible that both transmissivity and thermal noise are probabilistic and described within a probability density function  $F(\tau, \bar{n})$ . Typically, thermal noise can always be considered constant by either assuming stable operational conditions, or by minimizing (maximizing) its potential value for best-case (worst-case) rates. This allows us to consider the simpler ensemble  $\mathcal{E}_F(\eta, \bar{n}) = \{F(\tau); \mathcal{E}_{\tau, \bar{n}}\}$  on which we place the following upper bound of its capacity [32,33],

$$\mathcal{C}[\mathcal{E}_F(\eta, \bar{n})] \leq \mathcal{L}_F(\eta, \bar{n}) := \int_{\bar{n}}^{\eta} d\tau F(\tau) \mathcal{L}(\tau, \bar{n}). \quad (6)$$

Here we define  $\mathcal{L}_F(\eta, \bar{n})$  as a tight capacity bounding function for thermal-lossy fading channels [40]. Intuitively, one can never outperform the pure-loss PLOB bound in the presence of thermal noise, hence we can always write

$$\mathcal{C}[\mathcal{E}_F(\eta, \bar{n})] \leq \mathcal{L}_F(\eta, \bar{n}) \leq \mathcal{B}_F(\eta). \quad (7)$$

## 2. Capacities of fading networks

We can combine the theory from these previous sections in order to provide a general model for quantum networks with fading channels. Indeed, we may construct a quantum network  $\mathcal{N} = (P, E)$  such that all edges  $(\mathbf{x}, \mathbf{y}) \in E$  are generally associated with a unique thermal-lossy fading channel,

$$\mathcal{E}_{\mathbf{x}\mathbf{y}} = \mathcal{E}_{F_{\mathbf{x}\mathbf{y}}}(\eta_{\mathbf{x}\mathbf{y}}, \bar{n}_{\mathbf{x}\mathbf{y}}), \quad \forall (\mathbf{x}, \mathbf{y}) \in E. \quad (8)$$

In this way, each network edge not only possesses a unique maximum transmissivity  $\eta_{\mathbf{x}\mathbf{y}}$  and thermal-noise properties

$\bar{n}_{\mathbf{x}\mathbf{y}}$ , but also a unique instantaneous transmissivity probability density function  $F_{\mathbf{x}\mathbf{y}}$  through which each edge can adopt its own fading dynamics (or lack thereof). This allows for a description of network channels within different environmental media such as fiber channels, ground-based free-space channels, or free-space channels beyond the atmosphere. Furthermore, we can retrieve pure-loss fading channels via  $\bar{n}_{\mathbf{x}\mathbf{y}} = 0$ .

It has been shown that the capacities of quantum networks can be derived through a combination of quantum-information theoretic tools and ideas from classical network theory [11]. By transforming the notion of classical network cuts into entanglement cuts of a quantum network, one can determine compact, analytical expressions for the network capacities of arbitrary architectures. Consider a pair of end users within the fading network  $\alpha, \beta \in P$ . We define an entanglement cut  $C$  as a means of disconnecting and partitioning the network into two disjoint superusers  $\mathbf{A}$  and  $\mathbf{B}$  such that  $\alpha \in \mathbf{A}$  and  $\beta \in \mathbf{B}$  and  $P = \mathbf{A} \cup \mathbf{B}$ . A network cut  $C$  generates an associated cut set,

$$\tilde{C} = \{(\mathbf{x}, \mathbf{y}) \in E | \mathbf{x} \in \mathbf{A}, \mathbf{y} \in \mathbf{B}\}, \quad (9)$$

defining a collection of network edges, which when removed successfully partitions the network.

As discussed in previous sections, single-path routing can be thought of as a generalization of repeater chains, where end-to-end communication is established via the sequential exchange of quantum systems along a designated path. The single-path network capacity  $\mathcal{C}^s(\mathcal{N})$  is bounded by determining the network cut  $C_{\min}$  that generates the smallest, maximum single-edge capacity in the cut set. For lossy and thermal-lossy fading networks, we may define the single-path capacity quantities [11],

$$\mathcal{B}^s(\mathcal{N}) := \min_C \max_{(\mathbf{x}, \mathbf{y}) \in \tilde{C}} \mathcal{B}_{F_{\mathbf{x}\mathbf{y}}}(\eta_{\mathbf{x}\mathbf{y}}), \quad (10)$$

$$\mathcal{L}^s(\mathcal{N}) := \min_C \max_{(\mathbf{x}, \mathbf{y}) \in \tilde{C}} \mathcal{L}_{F_{\mathbf{x}\mathbf{y}}}(\eta_{\mathbf{x}\mathbf{y}}, \bar{n}_{\mathbf{x}\mathbf{y}}), \quad (11)$$

which upper bound the single-path network capacity,

$$\mathcal{C}^s(\mathcal{N}) \leq \mathcal{L}^s(\mathcal{N}) \leq \mathcal{B}^s(\mathcal{N}). \quad (12)$$

In the absence of thermal noise, the single-path capacity  $\mathcal{B}^s(\mathcal{N})$  is achievable and equates to performing sequential communication along the optimal route  $\omega^*$  in the network. For an arbitrary network, finding the optimal route is equivalent to solving the well-known widest-path problem and can be solved efficiently [41]. It is unknown whether the thermal upper bound in Eq. (6) is achievable, hence in the presence of thermal noise  $\mathcal{L}^s(\mathcal{N})$  presents a tight upper bound.

More powerful network protocols employ multipath routing [42]. The multipath network capacity is associated

with an optimal flooding protocol, and is found by locating the entanglement cut  $C_{\min}$ , which minimizes the multi-edge capacity over all cut sets. For lossy and thermal-lossy fading networks we can compute the multipath quantities [11],

$$\mathcal{B}^m(\mathcal{N}) := \min_C \sum_{(x,y) \in \bar{C}} \mathcal{B}_{F_{xy}}(\eta_{xy}), \quad (13)$$

$$\mathcal{L}^m(\mathcal{N}) := \min_C \sum_{(x,y) \in \bar{C}} \mathcal{L}_{F_{xy}}(\eta_{xy}, \bar{n}_{xy}), \quad (14)$$

which upper bound the multipath network capacity,

$$\mathcal{C}^m(\mathcal{N}) \leq \mathcal{L}^m(\mathcal{N}) \leq \mathcal{B}^m(\mathcal{N}). \quad (15)$$

Once more, for pure-loss-based networks the flooding capacity  $\mathcal{B}^m(\mathcal{N})$  is achievable, and equates to solving the classical maximum-flow minimum-cut problem according to a network of capacity achieving links. For general quantum networks with an arbitrary architectures, this problem requires a numerical treatment and can be solved efficiently [43–45]. Once more, since the thermal-loss upper bound is not guaranteed to be achievable  $\mathcal{L}^m(\mathcal{N})$  is instead a tight upper bound.

### C. Free-space quantum communication

Consider two remote parties Alice and Bob who are separated by a distance  $z$ , and employ quantum communications based upon a quasimonochromatic optical mode ( $\Delta\lambda$ -nm large and  $\Delta t$ -s long). This may be characterized by a Gaussian beam with wavelength  $\lambda$ , initial field spot size  $w_0$ , and curvature  $R_0$ . Communication consists of transmitting a directed beam towards a receiver with circular aperture of radius  $a_R$ . Here we assume that the initial spot size  $w_0$  is sufficiently small with respect to the transmitter aperture of radius  $a_T$  so that there is no relevant diffraction caused by the transmitter.

The atmospheric effects, which characterize free-space channels, are variable with respect to altitude, due to changes in atmospheric density. Therefore, specifying the trajectory of a Gaussian beam through free space is pivotal in capturing channel quality. To this end, for any point-to-point communications task we may assume a general beam trajectory  $L$  and introduce the following altitude and propagation functions, respectively,  $h_L(z)$  and  $z_L(h)$ . Using these functions we can retain a geometry independent framework for our study until we wish to specify to a particular setting.

#### 1. Free-space transmissivity

Free-space diffraction is a universal contributor to loss. As a beam propagates in free space its waist will widen as

a function of the distance it travels,

$$w_d^2(z) = w_0^2 \left[ \left( 1 - \left( \frac{z}{R_0} \right)^2 \right) + \left( \frac{z}{z_R} \right)^2 \right], \quad (16)$$

where  $z_R := \pi w_0^2 / \lambda$  is the Rayleigh range. A target receiver will then detect only a portion of the spread beam since its aperture is finite in size, inducing a diffraction-limited transmissivity,

$$\eta_d(z) = 1 - \exp \left[ - \frac{2a_R^2}{w_d^2} \right]. \quad (17)$$

It is also useful to define a diffraction-induced transmissivity in the far-field regime,  $z \gg z_R$ , making the approximation  $\eta_d \approx \eta_d^{\text{far}} := 2a_R^2 / w_d^2$ . This loss quantity exists regardless of the specific environmental setting considered, from ground-based links to intersatellite connections.

Propagation through the atmosphere incurs further loss due to aerosol absorption and Rayleigh-Mie scattering; an effect known as atmospheric extinction. At a fixed altitude  $h$ , this loss can be accurately described via the Beer-Lambert equation [27]. Since beam trajectories may be variable in altitude, we can generally define the extinction-induced transmissivity as

$$\eta_{\text{atm}}(z) = \exp \left[ - \int_0^z dz \alpha [h_L(z)] \right], \quad (18)$$

where  $\alpha(h) = \alpha_0 e^{-h/\bar{h}}$  is the extinction factor,  $\bar{h} = 6600$  m, and  $\alpha_0$  is the extinction factor at sea level. For  $\lambda = 800$  nm it follows that  $\alpha_0 \approx 5 \times 10^{-6} \text{ m}^{-1}$ .

Finally, there exist inevitable internal losses associated with the detector setup, due to imperfect fiber couplings, suboptimal quantum detector efficiency, and more. This inefficiency-induced transmissivity can be as low as  $\eta_{\text{eff}} \approx 0.4$  and must be considered to capture realistic performance. All of these effects can be used to describe a fixed, maximum transmissivity of a free-space connection,

$$\eta(z) := \eta_{\text{eff}} \eta_{\text{atm}}(z) \eta_d(z). \quad (19)$$

Of note,  $\eta$  can be readily modified to consider variable altitude beam trajectories and written as a function of a chosen spatial geometry to account for different extinction properties throughout the atmosphere.

#### 2. Atmospheric fading

It is remarkably optimistic to assume that a free-space transmission deterministically undergoes a pure-loss channel characterized by Eq. (19) only. The chaotic behavior of air flow, temperature and pressure throughout the atmosphere invites further complications for free-space transmissions, causing inaccuracies in the point-to-point

trajectory known as *beam wandering*. As a result, we must incorporate fading for a more accurate characterization.

Turbulence is used to describe how a free-space propagating beam is perturbed by fluctuations in the atmospheric refractive index, caused by spatial variations in pressure and temperature. Propagating beams interact with small turbulent air flows on a fast time scale, too fast for communicators to monitor or resolve. This causes the beam waist to broaden and forces us to define a *short-term spot size*  $w_{\text{ST}}$ , which is larger than the diffraction-induced spot size,  $w_d < w_{\text{ST}}$ . On a slower time scale, the beam will undergo deflections by significantly larger eddies in the atmosphere. This slower time scale may be reconcilable by the communicators, and manifests as a wandering of the beam centroid. This wandering can be described by a Gaussian random walk of the centroid with variance  $\sigma_t^2$ , which is a functional of the beam trajectory, operational setup, conditions, and more.

Wandering is not exclusively caused by turbulence, and one must also consider pointing errors caused by jitter and imperfect targeting. These effects also occur on a reasonably slow time scale of order  $0.1 - 1$  s, and may be resolved by the receiver. This introduces an additional wandering variance  $\sigma_p^2$ , e.g., a  $1\text{-}\mu\text{rad}$  pointing error at the transmitter causes a variance  $\sigma_p^2 \approx (10^{-6}z)^2$  (where  $z$  is in meters). Overall, these effects combine to induce Gaussian centroid wandering with variance  $\sigma^2 = \sigma_t^2 + \sigma_p^2$ .

The ability for communicators to resolve these wandering dynamics is dependent on their time scale. The behavior of turbulence is variable, with regimes ranging from weak to strong turbulence. Increasing turbulent strength can be modeled as an increasingly faster fading process, such that a receiver loses the ability to reconcile the wandering dynamics. For stronger levels of turbulence, it is possible to define a *long-term spot size*  $w_{\text{LT}}$ , which averages over the wandering caused by both small turbulent eddies and larger eddy deflections,  $w_d < w_{\text{ST}} < w_{\text{LT}}$ . Indeed, the turbulence-induced variance is defined with respect to the long-term and short-term quantities  $\sigma_t^2 = w_{\text{LT}}^2 - w_{\text{ST}}^2$ . However, rigorous studies of strong turbulence will require further considerations, for which work is currently underway [46].

In this work, we focus on the regime of weak turbulence and the concept of short-term beam spot sizes. These can be used to provide precise descriptions of free-space quantum channels on the ground at short range, and for ground-to-satellite communication along trajectories with small zenith angles [32,47,48].

### 3. Weak turbulence

For communications undergoing weak turbulence, the beam wandering acts on a time scale of  $10\text{--}100$  ms and can be fully resolved with a sufficiently fast detector. In

this case, analytical expressions can be found for the short-term spot size  $w_{\text{ST}}$  and the centroid wandering variance  $\sigma^2$ . Consider a beam with wave number  $k = 2\pi/\lambda$  following a free-space trajectory  $L$  [and its associated altitude function  $h_L(z)$ ]. Then the spherical-wave coherence length is given by,

$$\rho_0(L) = \left[ 1.46k^2 \int_0^z d\zeta \left( 1 - \frac{\zeta}{z} \right)^{5/3} C_n^2[h_L(\zeta)] \right]^{-3/5}, \quad (20)$$

where  $C_n^2$  denotes the refractive-index structure constant, used to measure the strength of fluctuations in the atmospheric refractive index. This quantity has an explicit dependence on the beam's trajectory, since this may be variable in altitude, and is typically described via the Hufnagel-Valley model (see Appendix C of Ref. [32]). Provided that Yura's condition is satisfied  $\phi := 0.33(\rho_0/w_0)^{1/3} \ll 1$  [49] then we can write [32],

$$w_{\text{ST}}^2 \approx w_d^2 + 2 \left( \frac{\lambda z}{\pi \rho_0} \right)^2 (1 - \phi)^2, \quad (21)$$

$$\sigma_t^2 \approx 2 \left( \frac{\lambda z}{\pi \rho_0} \right)^2 [1 - (1 - \phi)^2]. \quad (22)$$

The short-term spot size can be used to update the diffraction-induced transmissivity to account for fast beam interaction with small turbulent eddies in the atmosphere. That is,

$$\eta_{\text{ST}} := 1 - \exp \left[ -\frac{2a_R^2}{w_{\text{ST}}^2} \right] \underset{z \gg z_R}{\approx} \eta_{\text{ST}}^{\text{far}} := \frac{2a_R^2}{w_{\text{ST}}^2}, \quad (23)$$

where we simultaneously introduce a far-field approximation,  $\eta_{\text{ST}}^{\text{far}}$  when the propagation distance is very large  $z \gg z_R$ .

Updating the diffraction-induced transmissivity in Eq. (19), we may write an alternative maximum transmissivity incorporating weakly turbulent effects,  $\eta = \eta_{\text{eff}} \eta_{\text{atm}} \eta_{\text{ST}}$ . This represents the optimal transmissivity parameter that can be achieved when the beam centroid  $\vec{x}_C$  is perfectly aligned with the receiver centroid  $\vec{x}_R$ , i.e., the centroid deflection is  $r := \|\vec{x}_C - \vec{x}_R\| = 0$ . However, due to turbulence and pointing errors, the beam centroid now undergoes a Gaussian random walk with variance  $\sigma^2$ , invoking a fading channel. We can then connect the nonzero centroid deflection  $r \geq 0$  to an instantaneous transmissivity  $\tau(r)$  to precisely capture the fading process. Gaussian wandering induces a Weibull distribution for the centroid deflection, which results in an instantaneous transmissivity probability density function  $F_\sigma[\tau(r)]$  [32]. Defining the

functions,

$$f_0(x) := [1 - \exp(-2x)I_0(2x)]^{-1}, \quad (24)$$

$$f_1(x) := \exp(-2x)I_1(2x), \quad (25)$$

where  $I_n$  is the modified Bessel function for  $n = 0, 1$ , we can introduce the following shape and scale parameters:

$$\gamma = \frac{4\eta_{\text{ST}}^{\text{far}}f_0(\eta_{\text{ST}}^{\text{far}})f_1(\eta_{\text{ST}}^{\text{far}})}{\ln[2\eta_{\text{ST}}f_0(\eta_{\text{ST}}^{\text{far}})]}, r_0 = \frac{a_R}{\ln[2\eta_{\text{ST}}f_0(\eta_{\text{ST}}^{\text{far}})]^{\frac{1}{\gamma}}}. \quad (26)$$

With these, we can now write the instantaneous transmissivity probability density function,

$$F_\sigma(\tau) = \frac{r_0^2}{\gamma\sigma^2\tau} \ln\left(\frac{\eta}{\tau}\right)^{\frac{2}{\gamma}-1} \exp\left[-\frac{r_0^2}{2\sigma^2} \ln\left(\frac{\eta}{\tau}\right)^{\frac{2}{\gamma}}\right]. \quad (27)$$

Consequently, we are left with a free-space, lossy-fading channel  $\mathcal{E}_{F_\sigma}(\eta) = \{F_\sigma(\tau); \mathcal{E}_\tau\}$ . Using the tools from Sec. II, we can study the capacities of free-space connections.

Hence, the capacities for free-space quantum communications (entanglement distribution or secret-key distribution) are upper bounded according to [32]

$$\mathcal{C} \leq \mathcal{B}_{F_\sigma}(\eta) = -\Delta(\eta, \sigma) \log(1 - \eta), \quad (28)$$

where  $\Delta$  represents a correction factor to the PLOB bound due to imperfect alignment,

$$\Delta(\eta, \sigma) = 1 + \frac{\eta}{\ln(1 - \eta)} \int_0^\infty dx \frac{\exp\left[\frac{-r_0^2}{2\sigma^2} x^{\frac{2}{\gamma}}\right]}{e^x - \eta}. \quad (29)$$

Through specification to a free-space trajectory, one can easily determine geometry-dependent expressions for this ultimate limit. Of note, for channels, which are accurately described as ensembles of pure-loss channels (thermal noise is negligible), then Eq. (28) is in fact an achievable and optimal rate,  $\mathcal{C} = \mathcal{B}_{F_\sigma}(\eta)$ . For all other scenarios where thermal noise is non-negligible, it remains an effective upper bound.

#### 4. Thermal noise

As discussed previously, pure-loss-based bounds remain ultimate bounds in the presence of thermal noise. Yet, it is still possible to construct tighter performance bounds by considering fading channels, which are ensembles of thermal-loss channels. Let  $\bar{n}_T$  be the mean number of input photons transmitted towards a receiver via a single free-space mode. For an instantaneous transmissivity  $\tau$  the mean photon number collected at the receiver will

be  $\bar{n}_R = \tau\bar{n}_T + \bar{n}$ , where  $\bar{n}$  describes the total environmental thermal noise added to the signal. It is useful to define contributions to this environmental noise via

$$\bar{n} := \eta_{\text{eff}}\bar{n}_B + \bar{n}_{\text{ex}}, \quad (30)$$

where the receiver collected  $\bar{n}_B$  mean background photons with detector efficiency  $\eta_{\text{eff}}$ , and  $\bar{n}_{\text{ex}}$  accounts for excess setup noise. In the study of ultimate limits,  $\bar{n}_{\text{ex}}$  can be considered to be approximately zero, or can be attributed to trusted noise.

For free-space links, the primary source of thermal noise is attributed to natural brightness within the field of view of the transmission, i.e., the sky, Sun, Moon, etc. Using a receiver of aperture  $a_R$ , angular field of view  $\Omega_{\text{FOV}}$ , a detector with time window  $\Delta t$  and frequency filter  $\Delta\lambda$  around  $\lambda$ , then the number of background thermal photons per mode is

$$\bar{n}_B = H_\lambda \Gamma_R, \text{ where } \Gamma_R := \Delta t \Delta\lambda \Omega_{\text{FOV}} a_R^2. \quad (31)$$

Here,  $H_\lambda$  describes the spectral irradiance of the environment in units of photons  $\text{m}^{-2} \text{s}^{-1} \text{nm}^{-1} \text{sr}^{-1}$ , and is unique to the operational setting and trajectory. Using the general bound from Eq. (6) and specifying to free-space beam wandering dynamics with variance  $\sigma^2$ , we can write the free-space thermal upper bound,

$$\mathcal{C} \leq \mathcal{L}_{F_\sigma}(\eta, \bar{n}) = \mathcal{B}_{F_\sigma}(\eta) - \mathcal{T}_{F_\sigma}(\eta, \bar{n}), \quad (32)$$

where the thermal correction is given explicitly by,

$$\begin{aligned} \mathcal{T}_{F_\sigma}(\eta, \bar{n}) := & \left[ 1 - \exp\left(\frac{-r_0^2}{2\sigma^2} \ln\left[\frac{\eta}{\bar{n}}\right]^{\frac{2}{\gamma}}\right) \right] \\ & \times \left[ \frac{\bar{n} \log_2(\bar{n})}{1 - \bar{n}} + h(\bar{n}) \right] - \mathcal{B}_{F_\sigma}(\bar{n}). \end{aligned} \quad (33)$$

This result applies to settings of weak and intermediate turbulence, such that one can substitute the appropriate reconcilable wandering variance and maximum transmissivity into this result.

#### 5. Noise suppression and frequency filters

As seen in Eq. (31), the number of background thermal photons per mode has a strong dependence on the frequency filter,  $\Delta\lambda$ . The frequency filter assists in blocking out noise, and thus the use of ultranarrow filters is highly desirable. In discrete-variable quantum communications, physical frequency filters are typically limited to around  $\Delta\lambda = 1 \text{ nm}$ . However, using continuous variable (CV) quantum systems and appropriate interferometric measurements it is possible to achieve much narrower effective filters.

Many CV-based protocols rely on the use of a local oscillator (or phase reference) in order to perform

homodyne or heterodyne measurements at the output. This phase reference may be co-propagated with signal pulses, or alternatively reconstructed at the receiver. This reconstruction method involves interleaving the signal pulses with strong reference pulses that carry information about the local oscillator [8]. Since the output of a homodyne measurements is proportional to the mean photon number in the local-oscillator modes, the ability to utilize bright references pulses over free-space channels introduces an *effective homodyne filter*. Thermal noise mode matching with the local oscillator and the signal will be detected, but all other noise will be filtered out. This allows for the implementation of ultranarrow effective filters on the order of  $\Delta\lambda = 0.1$  pm with practical CV protocols, and can dramatically reduce the magnitude of the thermal background noise (see Ref. [32] for more details).

## D. Useful free-space channels

### 1. Ground-based channels

Wireless classical communication networks are ubiquitous and fundamental to everyday modern life. Thus the desire for a free-space quantum analog is obvious, enabling access to future wireless quantum technologies. Nonetheless, it is intuitive that such communication will be limited to short-range thanks to prominent decoherence obtained at ground level. At a fixed altitude, beam trajectories are horizontal paths with the simple altitude and propagation functions  $h_L(z) = h$ ,  $z_L(h) = z$ . The absence of a variable altitude in the beam path simplifies a number of key quantities such as the extinction-induced transmissivity

$$\eta_{\text{atm}}(z) = \exp[-\alpha(h)z], \quad (34)$$

and the spherical-wave coherence length

$$\rho_0 = [0.548k^2 C_n^2(h)z]^{-3/5}, \quad (35)$$

which can be used to accurately describe decoherence and fading dynamics on the ground. Here, turbulence is a major factor and must be stringently considered. A useful parameter for assessing the validity of turbulent regimes on the ground is the Rytov variance,

$$\sigma_{\text{Ry}}^2 = 1.23 k^{7/6} z^{11/6} C_n^2(h). \quad (36)$$

In particular, weak turbulence requires that  $\sigma_{\text{Ry}}^2 \lesssim 1$ . Using a Gaussian beam with  $\lambda = 800$  nm and altitudes close to sea level during typical day-time conditions, weak turbulence is only guaranteed for distances of  $z \lesssim 1$  km. Beyond this, as in the intermediate ( $\sigma_{\text{Ry}}^2 \gtrsim 1$ ) and strong ( $\sigma_{\text{Ry}}^2 \gg 1$ ) turbulent regimes, the long-term spot size must be adopted, leading to poorer ultimate channel capacities [46].

Figure 1(a) illustrates the behavior of transmissivity in ground-based free-space channels with respect to propagation length. Within the weak-turbulence regime the

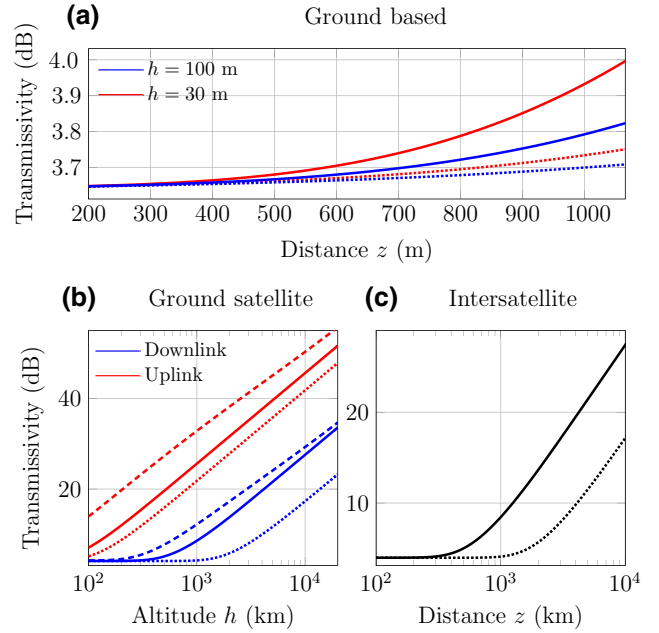


FIG. 1. Free-space transmissivity associated with (a) ground-based, (b) ground-satellite, and (c) intersatellite communication links. In each plot, solid lines depict the average transmissivity (attenuation averaged over fading dynamics), while dotted lines describe the best-case transmissivity (absence of fading). The dashed lines in (b) describe a ground-satellite free-space link with zenith angle  $\theta = 1$  radian, while the others consider  $\theta = 0$ . The operational setup in (a) is consistent with the parameters in Table II while (b),(c) are consistent with setup (1) in Table I.

loss properties of free-space channels limited to approximately 4 dB for communications over 1 km, encouraging the utility of short-range, optical free-space quantum communications.

For the assessment of thermal bounds, the primary source of thermal noise at ground level is attributed to the brightness of the sky. This provides a spectral irradiance ranging from

$$H_{\lambda}^{\text{sky}} \approx \begin{cases} 1.9 \times 10^{13}, & \text{full Moon, clear night,} \\ 1.9 \times 10^{18}, & \text{cloudy day time.} \end{cases} \quad (37)$$

in units of photons  $\text{m}^{-2} \text{s}^{-1} \text{nm}^{-1} \text{sr}^{-1}$ . Using this information, the expressions in Eqs. (34) and (35), and the general capacity bounds developed in the previous sections, we can accurately assess the ultimate limits of free-space quantum communications on the ground (see Ref. [32] for further details and derivations).

### 2. Ground-satellite channels

For communication between ground and satellite stations, there are two unique configurations that must be considered: transmissions directed from the ground towards

a satellite (uplink) or from a satellite towards the ground (downlink). The quantum channel descriptions of these configurations are very different.

Consider a Gaussian beam propagated in uplink. The beam immediately undergoes turbulence upon generation at low altitude, and thus has a large decohering impact, which must be carefully considered. However, pointing errors are less critical  $\sigma_p^2 \ll \sigma_i^2$  thanks to the availability of adaptive optics to optimize the beam trajectory from the ground station. Therefore we must model uplink as a fading channel predominantly due to turbulent effects. Meanwhile, a Gaussian beam in downlink experiences the opposite; the beam does not undergo serious levels of turbulence until it reaches lower altitudes. But by this point, its spot size has already been spread by diffraction, hence turbulence does not present a serious factor and  $\sigma_i^2 \approx 0$ . Yet, in this setting pointing errors become much more relevant due to the lack of onboard access and optimization ability. Hence, atmospheric decoherence associated with uplink and downlink is physically asymmetric, invoking two unique fading channels.

We specify the trajectory of ground-satellite communication according to a target satellite altitude  $h$  and zenith angle  $\theta$ , which describes the angle formed between the zenith point at the ground station and the direction of observation towards the satellite. The zenith angle takes values  $\theta \in [-\pi/2, \pi/2]$ , such that when  $\theta = 0$  the satellite is at the zenith. The distance that the beam physically travels from its point of generation  $z$  (known as its slant distance) can then be expressed with respect to this geometry. Defining the functions,

$$\begin{aligned} h_\theta(z) &= \sqrt{R_E^2 + z^2 + 2zR_E \cos \theta} - R_E, \\ z_\theta(h) &= \sqrt{h^2 + 2hR_E + R_E^2 \cos^2 \theta} - R_E \cos \theta. \end{aligned} \quad (38)$$

We may then introduce the altitude and propagation functions with respect to uplink and downlink communications [33],

$$z_\theta^{\text{up}}(h) = z_\theta(h), \quad z_\theta^{\text{down}}(h) = z_\theta(h_{\text{max}}) - z_\theta(h), \quad (39)$$

$$h_\theta^{\text{up}}(z) = h_\theta(z), \quad h_\theta^{\text{down}}(z) = h_\theta[z_\theta(h_{\text{max}}) - z]. \quad (40)$$

Figure 1(b) illustrates the behavior of transmissivity in ground-satellite channels with respect to uplink, downlink, and satellite altitude. Here we plot both the the expected transmissivity when averaged over the respective fading processes and maximum transmissivity (a best-case loss in the absence of fading). Crucially, it can be shown that for beam trajectories with relatively small zenith angles  $\theta \leq 1$  radian, we can assume the regime of weak turbulence for the ground-satellite fading channel (see Appendix C of Ref. [32]). Within this angular window we can accurately resolve the fading dynamics, and by inserting the

beam-trajectory expressions into the machinery of Sec. II C 2, it is possible to derive loss-based ultimate limits for both uplink and downlink quantum communications using Eq. (28), and thermal-loss-based limits using Eq. (32).

The sources of environmental thermal-noise are also unique to both uplink and downlink configurations, and operational settings such as the time of day and weather. In uplink during the day, the primary source of thermal noise is sunlight being reflected from the Earth to the satellite detector. Meanwhile, at night, this noise is diminished but there still exists sunlight being reflected from the Moon to the Earth, and back towards the satellite. For uplink, we may write

$$\bar{n}_B^{\text{up}} = \kappa H_\lambda^{\text{sun}} \Gamma_R. \quad (41)$$

Here  $\kappa$  is a parameter that accounts for the Earth and Moon albedos and ranges from  $\kappa_{\text{night}} = 7.36 \times 10^{-7}$  for a clear night with a full Moon, to  $\kappa_{\text{day}} = 0.3$  during clear day time. Meanwhile, for the optical wavelength  $\lambda = 800$  nm, we can approximate that in uplink the solar spectral irradiance is  $H_\lambda^{\text{sun}} = 4.61 \times 10^{18}$  photons  $\text{m}^{-2} \text{s}^{-1} \text{nm}^{-1} \text{sr}^{-1}$ .

For downlink, the receiver is now a detector on the ground and the main source of noise is more simply attributed to the sky (as it was in the ground-based scenario). In this setting, and for  $\lambda = 800$  nm, the spectral irradiance of the sky follows Eq. (37). For a much more detailed analysis, see Appendix D, Ref. [33].

### 3. Intersatellite channels

Finally, we can consider free-space quantum communication between satellites in orbit. This represents a high-quality free-space quantum channel, which is free from atmospheric decoherence, and thus will not experience losses due to extinction nor undergo turbulence. Indeed, these intersatellite link losses are characterized by free-space diffraction only. Assuming negligible pointing errors, then the intersatellite channel is simply a lossy channel with transmissivity given by  $\eta_d(z)$  as a function of the propagation distance between satellites,  $z$ . This lets us write an ideal upper bound on the intersatellite channel capacity,

$$\mathcal{C} \leq \mathcal{B}(\eta_d) = \frac{2a_R^2}{w_d^2(z) \ln 2}. \quad (42)$$

Due to the lack of onboard access and adaptive optics, it is possible that pointing errors become relevant and must be considered. If pointing errors are non-negligible,  $\sigma_p^2 > 0$ , then we instead must consider a lossy-fading channel  $\mathcal{E}_{F_{\sigma_p}} = \{F_{\sigma_p}; \mathcal{E}_\tau\}$  with maximum transmissivity  $\eta_d(z)$ . As discussed in earlier sections, pointing errors occur on a sufficiently slow time scale such that they are reconcilable by the receiver. Hence, the capacity for this channel can be

accessed via Eq. (28), such that

$$\mathcal{C} \leq \mathcal{B}_{F\sigma_p}(\eta_d) = \frac{2\alpha_R^2}{w_d^2(z) \ln 2} \Delta(\eta_d(z), \sigma_p), \quad (43)$$

where  $\Delta$  acts as a correction factor to the PLOB bound. It is clear that when  $\sigma_p^2 = 0$  we retrieve Eq. (42). In Fig. 1(c) the loss properties of an optical intersatellite channel are illustrated with respect to distance between communicating satellites. This depicts similar transmissivity behavior to ground-satellite downlink channels with zenith angle  $\theta = 0$  without the additional degradation associated with atmospheric interactions.

We have some considerations to note. First of all, intersatellite channels can only be formed between satellites that fall within each other's line of sight. This naturally implies a limit to the maximum distance over which an intersatellite channel can be physically established. For any two satellites in circular orbits, at some point the Earth blocks the free space between them, prohibiting transmittance. If two satellites orbit at altitudes  $h_1$  and  $h_2$ , then we find this limit to be

$$z_{\text{sight}}^{\text{max}} := \frac{h_1(h_1 + 2R_E)}{h_1 + R_E} + \frac{h_2(h_2 + 2R_E)}{h_2 + R_E}. \quad (44)$$

This is derived through basic geometric considerations (see the Supplemental Material for a derivation [51]).

Secondly, let us justify the modeling of intersatellite channels as pure-loss channels. The number of thermal photons impinging upon a satellite detector is determined by the orientation and field of view of the detector. For communication between satellites, the transmitters and detectors do not occupy fixed orientations with respect to the main sources of brightness. Indeed, there will exist best-case and worst-case orientations: in the best-case scenario, the satellite detector will face completely away from the Earth or Moon, so that their albedos are not within the detector's field of view whatsoever. In a worst-case scenario, the detector will be oriented directly facing the Earth (as in uplink).

However, point-to-point quantum communication can always be optimized by choosing the physically directed channel, which results in less thermal background photons at the detector; irrespective of the logical direction of communication. That is, each intersatellite channel can exchange quantum systems in the direction, which achieves the best detector orientation with respect to background noise. By optimizing the physical orientation of an intersatellite quantum network, each receiver will only ever experience a fraction of the worst background noise experienced by satellite uplink channels for which thermal corrections are minimal for link lengths of  $z \lesssim 10\,000$  km [33]. We leave more formal treatments of these channel properties to future works, with the confidence that pure-loss channels accurately model such free-space links.

Hence, we can reliably model intersatellite free-space links as pure-loss channels. As such, we treat the upper bound in Eq. (43) as an achievable rate so that  $\mathcal{C} = \mathcal{B}_{F\sigma_p}(\eta_d)$  can be accomplished by an optimal point-to-point protocol.

### III. MODULAR QUANTUM NETWORKS

#### A. Network model

In this work, we construct a simple model for the study of modular quantum networks. Namely, we consider a global network  $\mathcal{N} = (P, E)$ , which consists of a collection of subnetworks called *communities*, where the  $i$ th community is denoted by the undirected subgraph

$$\mathcal{N}_{c_i} = (P_{c_i}, E_{c_i}), \quad P_{c_i} \subset P, \quad E_{c_i} \subset E. \quad (45)$$

Here,  $P_{c_i}$  defines a subset of all network nodes that compose the  $i$ th community, while  $E_{c_i}$  denotes the subset of all network edges that connect them. For now, we consider each community network to be completely general, and can adopt an arbitrary topology. Here, we focus on quantum networks, which observe *spatial* modularity [50], such that communities are spatially separated. This means that each community is completely disconnected from every other community, i.e., the community node sets are all pairwise disjoint  $P_{c_i} \cap P_{c_j} = \emptyset$ , for all  $i, j$ .

In order to mediate communication between different communities, we introduce a *backbone network*  $\mathcal{N}_b = (P_b, E_b)$ . This is a large-scale network for which none of its nodes  $\mathbf{x} \in P_b$  are user nodes, used purely to facilitate end-to-end communications between users contained in different communities. Crucially, we assume that each community possesses a set of undirected edges, which connect a set of community nodes to backbone network nodes. We refer to these as *intercommunity edges*, such that the set of intercommunity edges

$$E_{c_i:b} := \{(\mathbf{x}, \mathbf{y}) \in E \mid \mathbf{x} \in P_{c_i}, \mathbf{y} \in P_b\}, \quad (46)$$

gives each community access to the backbone.

More precisely, we can define an intercommunity subnetwork  $\mathcal{N}_{c_i:b} = (P_{c_i:b}, E_{c_i:b})$ , which describe the undirected graph that emerges between the  $i$ th community and the backbone. The set  $P_{c_i:b}$  defines the complete collection of nodes that are interconnected between the community and the backbone. However, the nodes  $\mathbf{x} \in P_{c_i:b}$  are already contained within  $\mathcal{N}_{c_i}$  or  $\mathcal{N}_b$ ; hence, it is useful to distinguish between the community nodes and the backbone nodes, which comprise this subnetwork. For this, we introduce the notation

$$P_{c_i|b} := P_{c_i:b} \cap P_{c_i} \subseteq P_{c_i}, \quad (47)$$

$$P_{b|c_i} := P_{c_i:b} \cap P_b \subseteq P_b. \quad (48)$$

Intuitively,  $P_{c_i|b}$  can be thought of as the subset of nodes from the community  $P_{c_i}$  conditioned on being connected to  $\mathcal{N}_b$  (and vice versa for  $P_{b|c_i}$ ).

This modular structure takes a very intuitive form and is remarkably useful for modeling realistic, hybrid quantum networks. When an equivalence relation is enforced between nodes in similar communities, the network quotient graph can be viewed as a star network [51]. It allows us to completely separate communities and the backbone from one another. This makes it easier to compartmentalize different subnetwork structures, which may operate in completely different physical domains. Furthermore, it helps to derive independent network conditions on each of the subnetworks in accordance with some global objective. We summarize this architecture in the following definition, which has also been illustrated in Fig. 2(a).

**Definition 1: (Modular network):** A modular network  $\mathcal{N} = (P, E)$  is a network architecture constituent of  $n$  community subnetworks  $\{\mathcal{N}_{c_i}\}_{i=1}^n$ , and a backbone subnetwork  $\mathcal{N}_b$ . Each community subnetwork is connected to the backbone via a set of edges  $E_{c_i:b}$ , described by the intercommunity subnetworks  $\{\mathcal{N}_{c_i:b}\}_{i=1}^n$ , and there are no direct links between communities.

## B. Modular network capacities

As discussed in Sec. II, the optimal end-to-end performance within a quantum network is quantified by its multipath or *flooding capacity*  $\mathcal{C}^m(\mathcal{N})$ , which describes the optimal number of target bits that can be transmitted between end users per use of a flooding protocol. Any quantum network  $\mathcal{N} = (P, E)$ , including the modular designs introduced, can be represented by a global distribution of channels  $\{\mathcal{E}_{xy}\}_{(x,y) \in E}$  and a corresponding distribution of single-edge channel capacities  $\{\mathcal{C}_{xy}\}_{(x,y) \in E}$ , where  $\mathcal{C}_{xy} := \mathcal{C}(\mathcal{E}_{xy})$ . For general fading networks, it is always possible to use these distributions and the general expressions from Eqs. (13) and (14) in order to determine the flooding capacity.

However, the translation into a modular architecture means that there exist particular classes of network cuts, which are performed on different subnetworks. It becomes very useful to formally define a number of the multiedge capacities associated with these classes of cuts. In each of the following settings, we consider a pair of end users  $\{\alpha, \beta\}$  contained within remote communities of a generic, global modular network, i.e.,  $\alpha \in P_{c_\alpha}$  and  $\beta \in P_{c_\beta}$  such that  $c_\alpha \neq c_\beta$ . It is now useful to denote community subnetworks with respect to the end user that they contain, i.e., we may write  $c_\alpha$  and  $c_\beta$ , respectively. We assume each subnetwork to adopt arbitrary topologies and capacity distributions.

## 1. Local-community capacities

We define a *local-community cut*  $C_{c_j}$  as that which partitions two end users within the network by exclusively collecting edges within one of the user communities  $c_j$ , for either  $\mathbf{j} \in \{\alpha, \beta\}$ . That is, a local-community cut set takes the form  $\tilde{C}_{c_j} = \{(\mathbf{x}, \mathbf{y}) \in E_{c_j} \mid \mathbf{x} \in \mathbf{A}, \mathbf{y} \in \mathbf{B}\}$ . This restricted form of network cut will generate an associated multiedge capacity, which we label a *local-community capacity*,

$$\mathcal{C}_{c_j}^m := \min_{C_{c_j}} \sum_{(\mathbf{x}, \mathbf{y}) \in \tilde{C}_{c_j}} \mathcal{C}_{xy}. \quad (49)$$

For end-user nodes  $\mathbf{j}$ , which do not share a direct connection with the backbone (i.e.,  $\mathbf{j} \notin P_{c_j|b}$ ), then this form of restricted cut always exist.

However, if an end-user node does share a direction connection with the backbone, then a valid local-community cut will not exist. In this case it is never sufficient to remove edges solely from the community networks, and one must cut at least one edge from the set of intercommunity edges  $E_{c_i:b}$ . To this end, we must slightly modify the local-community cut so that it removes any direct connections from the user node to the backbone, and then to identify the optimal set of edges to be removed from the community. Hence, a valid cut set becomes  $\tilde{C}'_{c_j} = \{(\mathbf{j}, \mathbf{y}) \in E \mid \mathbf{y} \in P_b\} \cup \tilde{C}_{c_j}$ . We can then define an analogous local-community capacity according to this class of network cut.

## 2. Backbone capacities

A *backbone cut*  $C_b$  is a network cut that exclusively collects edges on the backbone network in order to partition the two end users. This kind of cut set takes the form  $\tilde{C}_b = \{(\mathbf{x}, \mathbf{y}) \in E_b \mid \mathbf{x} \in \mathbf{A}, \mathbf{y} \in \mathbf{B}\}$ , which generates an associated multiedge *backbone capacity*,

$$\mathcal{C}_b^m := \min_{C_b} \sum_{(\mathbf{x}, \mathbf{y}) \in \tilde{C}_b} \mathcal{C}_{xy}. \quad (50)$$

In the modular network architecture we are investigating, when considering end users contained in unique communities, these kinds of cuts always exist. It is always sufficient to perform a cut on the backbone since there does not exist any other collection of edges that can be used to form a valid path between communities.

## 3. Global-community capacities

Finally, we can formalize a multiedge capacity associated with exclusively collecting intercommunity edges. The end-user communities  $\mathcal{N}_{c_\alpha}$  and  $\mathcal{N}_{c_\beta}$  are connected to the backbone via the sets of intercommunity edges  $E_{c_\alpha:b}$  and  $E_{c_\beta:b}$ , respectively. If we remove either of these sets of

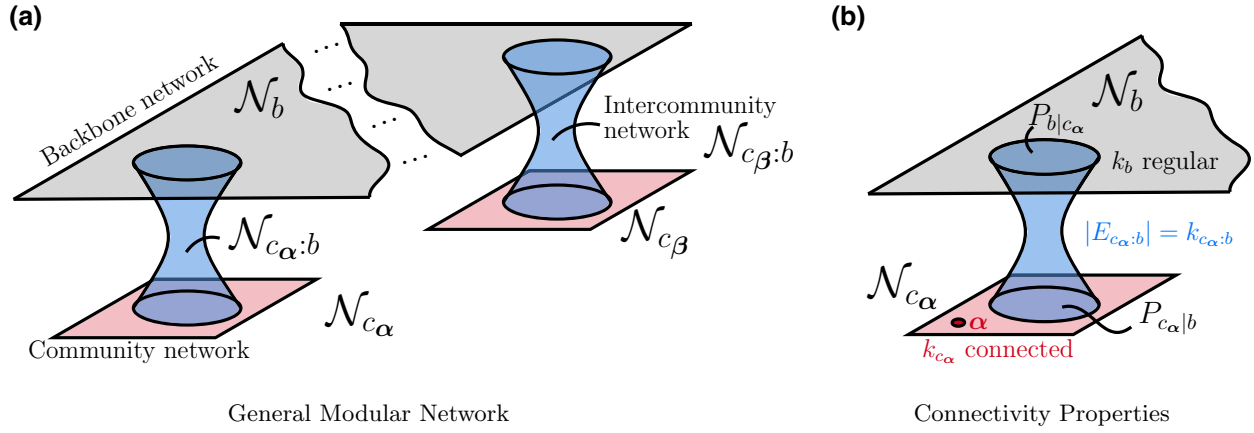


FIG. 2. (a) A modular quantum network architecture, constituted from community subnetworks  $\mathcal{N}_{c_\alpha}$ ,  $\mathcal{N}_{c_\beta}$ , and a backbone network  $\mathcal{N}_b$ . Each community is connected to the backbone via the subnetworks  $\mathcal{N}_{c_\alpha:b}$  and  $\mathcal{N}_{c_\beta:b}$ . Nodes from the community  $c_j$ , which are directly connected to the backbone, are contained in  $P_{c_j|b}$ , while the nodes in the backbone, which are connected to the community, are contained in  $P_{b|c_j}$ . (b) We may idealize this modular structure by placing ideal connectivity constraints on each of the subnetworks.

edges, then the two remote users would be automatically partitioned. Hence, the edge sets  $E_{c_\alpha:b}$  and  $E_{c_\beta:b}$  both correspond to valid cuts on the network and each generate a multiedge capacity

$$C_{c_j:b}^m := \sum_{(x,y) \in E_{c_j:b}} C_{xy}, \quad (51)$$

for  $\mathbf{j} \in \{\alpha, \beta\}$ . We can then minimize over the end users to define a multiedge capacity,

$$C_{c:b}^m := \min_{\mathbf{j} \in \{\alpha, \beta\}} C_{c_j:b}^m. \quad (52)$$

Clearly, this form of network cut always exists. We refer to this kind of partitioning as community isolation, since it isolates a community subnetwork entirely from the rest of the network. Furthermore, we name  $C_{c:b}^m$  the *global-community capacity*, as it refers to globally isolating the entire community subnetwork [52].

### C. Idealized modular networks

Arbitrary architectures can always be treated using the capacity expressions from Sec. II for general fading networks. However, the generality of these arguments make it difficult to present rigorous analytical statements about specific features or tangible network properties. In order to understand the ultimate potential of quantum networks, we need to simultaneously optimize the point-to-point channels and the network architecture in which they are arranged. Hence, it is desirable to strike a balance between realism and ideality in such a way that allows us to derive informative results about quantum networks and end-to-end performance. In the following we propose subnetwork connectivity constraints that strike this balance.

#### 1. Backbone regularity

Firstly, we can impose regularity on the network backbone, demanding that the degree of each node is constant. This leads to a highly connected network structure, which is ideal for multipath routing strategies. Let the function  $\deg(\mathbf{x})$  compute the degree of the node  $\mathbf{x}$ . Then we impose

$$\deg(\mathbf{x}) = k_b, \forall \mathbf{x} \in P_b, \quad (53)$$

which defines the regularity parameter of the backbone. It is worthwhile to make clear that these constraints apply only to intranetwork connections. Indeed, a node on the backbone can have  $k_b$  connections to neighbors on the backbone network, but also possess additional intercommunity connections via the subnetwork  $\mathcal{N}_{c_j:b}$ , without any further constraint. It is useful to quantify the number of intercommunity connections permitted between the backbone and communities using the notation,

$$k_{c_j:b} = |E_{c_j:b}|, \mathbf{j} \in \{\alpha, \beta\}. \quad (54)$$

While regularity is an idealized property of realistic networks, in the context of a nonuser repeater network such as the backbone it is very much feasible and extremely useful in order to understand the limits of quantum networks.

#### 2. Community connectivity

Community subnetworks are likely to be smaller scale and less predictable structures than the backbone, partly due to the presence of user nodes. Thus flexibility in their design is useful. Here, we do not impose regularity but instead define classes of communities in accordance with the smallest local-community cut that they contain.

**Definition 2:** (*k<sub>c</sub> connectivity*): Consider a community subnetwork  $\mathcal{N}_c$ . We say the community is  $k_c$  connected if

$k_c$  is the smallest number of edges that must be removed in order to disconnect a pair of community nodes, minimized over all possible node pairs  $\mathbf{x} \neq \mathbf{y} \in P_c$ . More precisely,

$$k_c := \min_{\mathbf{x} \neq \mathbf{y} \in P_c} |\tilde{C}_c|, \quad (55)$$

where  $\tilde{C}_c$  denotes a community cut set between the nodes  $\mathbf{x}$  and  $\mathbf{y}$ .

Hence,  $k_c$  defines the minimum local community cut-set cardinality, given some network topology and choice of end users. This is a completely general property, which is unique for all community networks, using the most easily disconnected pair of nodes in the network as a metric for how well it is connected. Regular networks are an example of an architecture for which their  $k_c$  connectivity is simply equal to the network regularity. Hence, we can consider community subnetworks to be  $k_c$  connected while encompassing a very large set of architectures.

### 3. Idealized modular network

Combining the constraints of regularity on the backbone and  $k_c$  connectivity on the community subnetworks, it is possible to define an ideal modular quantum network architecture in terms of these parameters. This generates a structure that can be investigated analytically in the following sections.

**Definition 3:** (*Ideal modular network*): An ideal modular network  $\mathcal{N}^* = (P, E)$  is a network architecture constituent of  $n$  community subnetworks  $\{\mathcal{N}_{c_i}\}_{i=1}^n$  each of which are  $k_{c_i}$  connected, and a backbone subnetwork  $\mathcal{N}_b$ , which is  $k_b$  regular. Each community subnetwork is connected to the backbone via  $k_{c_i:b}$  edges, described by the intercommunity subnetworks  $\{\mathcal{N}_{c_i:b}\}_{i=1}^n$ , and there are no direct links between communities.

An illustration of this architecture can be found in Fig. 2(b). When focusing on a particular pair of end-user nodes  $\{\alpha, \beta\}$  from two remote communities in the global network, we can then specify their  $k_{c_j}$ -connectivity properties.

#### D. Minimum cut as community isolation

Care must be taken when constructing this form of modular network to ensure not only high-rate communication within each community, but also high-rate communication between different communities mediated by the backbone. If the backbone network is poorly connected, or possesses weak links, it will not effectively assist long-distance communication. Meanwhile, even if communities are connected to a high-quality backbone, insufficiently strong capacities in a local community can compromise its use. Hence, there exists a careful balance between all of the subnetworks in the modular model, and their connectivity and capacity properties throughout. It is therefore highly

desirable to identify a relationship between the quality of channels within the backbone and the quality of channels within the communities.

In order to better grasp these relationships, we can investigate the ideal modular networks  $\mathcal{N}^*$  defined in Definition 3. Regular networks (such as that on the backbone) possess very convenient qualities, which allow for useful insight into minimum network cuts. As such, they can be analytically studied as highly connected, ideal network structures and used to reveal fundamental limitations for end-to-end communication.

Our mission becomes the following: to derive conditions on each of the subnetworks such that the flooding capacity between the remote users is always their global-community capacity. In this way, the minimum cut is always achieved by community isolation on either of the end-user communities. Equivalently, it means that the minimum cut can always be found on a simplified quotient graph of the modular network, vastly simplifying its analysis [40]. When this is the case, the end-to-end capacities between any two unique communities are always *distance independent*, i.e., the ultimate rate between two end-user communities does not change with respect to the physical separation of those communities. This is an extremely desirable property of a quantum network, particularly on large scales.

If a modular network satisfies this property, it means that (i) the backbone network is of sufficiently high quality that it never impedes the network performance over (potentially very) long distances, and (ii) that the local communities are of sufficiently high quality that neither compromises local or network-wide communication. Furthermore, by imposing that the minimum cut be the intercommunity edges, it allows us to reveal unique constraints on each subnetwork, which are summarized in the following theorem.

**Theorem 1.** Consider an ideal modular network of the form  $\mathcal{N}^*$  introduced in Definition 3. Select any pair of end users  $\{\alpha, \beta\}$  contained in remote communities  $\alpha \in P_{c_\alpha}$  and  $\beta \in P_{c_\beta}$ . For all  $\mathbf{j} \in \{\alpha, \beta\}$ , there exist single-edge threshold capacities on the communities  $C_{c_j}^{\min}$  and backbone  $C_b^{\min}$  subnetworks for which the network flooding capacity is given by the global-community capacity,

$$\left. \begin{aligned} C_{\mathbf{xy}} &\geq C_{c_j}^{\min}, \forall (\mathbf{x}, \mathbf{y}) \in E_{c_j}, \\ C_{\mathbf{xy}} &\geq C_b^{\min}, \forall (\mathbf{x}, \mathbf{y}) \in E_b, \end{aligned} \right\} \implies C^m(\mathcal{N}) = C_{c:b}^m. \quad (56)$$

The threshold capacities are given by,

$$C_{c_j}^{\min} := \frac{C_{c:b}^m}{k_{c_j}}, \quad C_b^{\min} := \frac{C_{c:b}^m}{H_{\min}^*}, \quad (57)$$

where  $H_{\min}^*$  is the minimum cut-set cardinality on the backbone network. If these threshold capacities are violated,

then the global-community capacity becomes an upper bound on the end-to-end capacity,  $\mathcal{C}^m(\mathcal{N}) \leq \mathcal{C}_{c,b}^m$ .

A detailed proof can be found in Sec. I of the Supplemental Material [51]. Thanks to backbone regularity and community connectivity, the minimum cut-set cardinalities that occur within each subnetwork can be easily identified. Then, it is straightforward to enforce single-edge capacity constraints, which ensure that the local-community and backbone capacities are always larger than the global-community capacity.

In this theorem, we use the fact that the cardinality of the smallest backbone cut set between two end users in remote communities can be analytically derived, thanks to network regularity. This minimum cardinality takes the form

$$H_{\min}^* := \min_{\mathbf{j} \in \{\alpha, \beta\}} H_{\min}(k_b, P_{b|c_j}), \quad (58)$$

where  $H_{\min}(k_b, P_{b|c_j})$  is a function that computes the minimum number of edges that must be cut to isolate all the nodes  $P_{b|c_j}$  on the backbone, which are also connected to the community  $c_j$ . The explicit form of this expression can be found in the Supplemental Material [51], and depends on the precise spatial arrangement of connections from the community to the backbone. However, we can generally bound this quantity using

$$k_b \leq H_{\min}(k_b, P_{b|c_j}) \leq k_b |P_{b|c_j}|. \quad (59)$$

The lower bound  $k_b$  corresponds to a worst-case spatial distribution of community-to-backbone connections, when all the community nodes are connected to the same node on the backbone, i.e.,  $|P_{b|c_j}| = 1$ . Then it is sufficient to isolate just one backbone node to perform a valid end-user cut, collecting only  $k_b$  edges (since the backbone is  $k_b$  regular). The upper bound corresponds to a best-case scenario; when all the community nodes are connected to backbone nodes, which do not share any neighbors or edges. In this case, the smallest cut set restricted to the backbone is found by isolating all nodes individually. As a result, this cut collects exactly  $k_b |P_{b|c_j}|$  edges.

Figure 3 depicts a number of examples of minimum backbone cut sets for remote communities connected to a Manhattan backbone ( $k_b = 4$ ). In these figures we display only one end-user community and assume that the other end-user community is sufficiently distant that it does not share intercommunity connected nodes on the backbone.

As a result, we can always present a best- and worst-case single-edge threshold capacity for the backbone network,  $\mathcal{C}_b^{\min}$ . That is, we can sandwich the backbone threshold

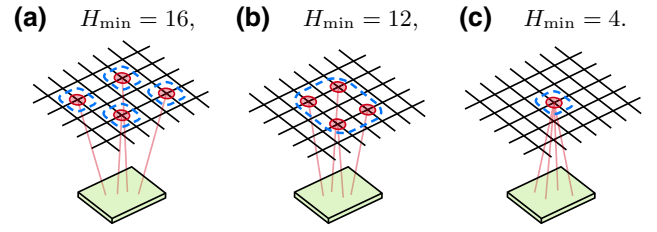


FIG. 3. Examples of minimum cardinality intercommunity cut sets for connections from an arbitrary community to a Manhattan backbone network ( $k_b = 4$ ). These are valid cuts, which isolate remote communities (only one community is illustrated here), and are performed exclusively on the backbone. Panel (a) captures the best-case spatial distribution of the largest potential cut set when no target nodes share any edges or neighbors, (b) illustrates an example in which neighbor sharing can diminish the overall cut-set size, and (c) describes the worst-case spatial distribution that minimizes the cut-set size.

capacity according to

$$\frac{\mathcal{C}_{c,b}^m}{k_b |P_{b|c_j}|} \leq \mathcal{C}_b^{\min} \leq \frac{\mathcal{C}_{c,b}^m}{k_b}, \quad \mathbf{j} \in \{\alpha, \beta\}. \quad (60)$$

The more effectively that the intercommunity connections are dispersed across the backbone, the weaker the single-edge constraint that must be forced upon it.

## IV. HYBRID FREE-SPACE NETWORKS

In this final section we combine results and theory from Secs. II and III in order to investigate hybrid fiber and free-space modular quantum networks. Here we study two pertinent cases in an effort to reveal tangible resource requirements for future quantum networks: A fiber and satellite modular configuration and a ground-based free-space and fiber model.

### A. Fiber and satellite configuration

#### 1. Motivation

An interesting modular configuration consists of fiber-based community networks, which are interconnected via a backbone satellite network. This model captures a realistic satellite-based model of the quantum internet, in which dynamic intersatellite links are used to facilitate long-distance quantum communication at high rates. In this scenario, the weakest links are typically the ground-to-satellite free-space connections, due to the impact of atmospheric decoherence and turbulence on a transmitted beam. Therefore, the constraints revealed in Theorem 1 are very realistic, as community isolation is likely to be the minimum cut in many settings.

In Theorem 1 we devise single-edge capacity lower bounds on the community networks, which guarantee the network flooding capacity is equal to the global-community capacity. For fiber-based networks, these

single-edge lower bounds can be used to identify a *maximum tolerable fiber length*,  $d_{c_j}^{\max}$  that is permitted within the fiber network. In the context of a satellite-based backbone network, the single-edge capacity lower bound can be translated into a *maximum intersatellite separation*,  $z_b^{\max}$ , which describes the maximum propagation distance that is permitted for free-space channels between satellites in the backbone. These are critical quantities, which directly motivate the construction of ground-based and satellite-based networks for global quantum communication.

## 2. Optimal performance

We wish to enforce that the minimum cut is always achieved by community isolation, generating the global-community capacity  $C^m(\mathcal{N}) = C_{c:b}^m$ . In this physical setting, each intercommunity edge is described by ground-to-satellite channel, which may be an uplink or downlink channel. Thanks to teleportation, a network protocol can always choose the physical channel direction that maximizes its point-to-point capacity independently from the desired logical direction of community. Downlink channels are always superior to uplink, and therefore we can simply model the global community capacity as the sum of a downlink capacities. This multiedge capacity will be bounded by

$$C_{c:b}^m \leq \min_{j \in \{\alpha, \beta\}} \sum_{(x,y) \in E_{c_j:b}} \mathcal{L}_{F_{xy}}(\eta_{xy}, \bar{n}_j), \quad (61)$$

$$\leq \min_{j \in \{\alpha, \beta\}} \sum_{(x,y) \in E_{c_j:b}} \mathcal{B}_{F_{xy}}(\eta_{xy}). \quad (62)$$

where  $F_{xy}$  and  $\eta_{xy}$  capture the fading dynamics and maximum transmissivity of each downlink channel that connect  $c_j$  to the backbone, and depend on beam trajectory. Meanwhile,  $\bar{n}_j$  infers community-wide thermal-noise conditions. Since all of the intercommunity edges in  $E_{c_j:b}$  are connected to a relatively small area, we can assume identical operational conditions for all downlink edges. However, these operational conditions will not be consistent for both end users; when communicating on a global scale, one user may be in night time while the other is in day time with independent weather conditions.

We can derive single-link distance constraints, which guarantee  $C_{c:b}^m$  to be the optimal network capacity. These conditions follow directly from Theorem 1 and are summarized in the following corollary:

**Corollary 2.** *Consider an ideal modular network of the form  $\mathcal{N}^*$  introduced in Definition 3, and assume optical-fiber community networks  $\mathcal{N}_{c_\alpha}$ ,  $\mathcal{N}_{c_\beta}$ , and a satellite-based backbone  $\mathcal{N}_b$ . Select any pair of end users  $\{\alpha, \beta\}$  located in remote communities  $\alpha \in P_{c_\alpha}$  and  $\beta \in P_{c_\beta}$ . There exists*

*a maximum fiber length in each community*

$$d_{c_j}^{\max} := -\frac{1}{\gamma} \log_{10} \left( 1 - 2^{-C_{c:b}^m/kc_j} \right), \quad (63)$$

*and a maximum intersatellite separation in the backbone*

$$z_b^{\max} := \arg \min_z \left| \log \left( \frac{H_{\min}^* \mathcal{B}_{F_{\sigma p}}(\eta)}{C_{c:b}^m} \right) \right|. \quad (64)$$

*for which the network flooding capacity is equal to the global-community capacity,*

$$C^m(\mathcal{N}) = C_{c:b}^m. \quad (65)$$

*Otherwise, if any intersatellite links violate this condition  $\exists z_{xy} > z_b^{\max}$ ,  $(x, y) \in E_b$  or the local community links are in violation,  $\exists d_{xy} > d_{c_j}^{\max}$ ,  $(x, y) \in E_{c_j}$ , for either  $j \in \{\alpha, \beta\}$ , then this becomes an upper bound on the network flooding capacity,  $C^m(\mathcal{N}) \leq C_{c:b}^m$ .*

The analytical simplicity of the maximum fiber length follows from the remarkably compact PLOB bound for bosonic lossy channels. However, the maximum intersatellite separation in Eq. (64) must be computed numerically due to the more complex PLOB bound, which accounts for fading due to pointing errors. The lack of onboard access makes it difficult to perfectly optimize beam trajectory, and thus pointing errors cannot be ignored. However, it is possible to analytically upper and lower bound the quantity  $z_b^{\max}$ .

An upper bound is found by considering a lack of pointing errors, which means the channel is no longer a fading channel but is instead a fixed lossy channel with the maximum possible transmissivity. This idealizes the intersatellite channel by removing the potential for beam wandering, resulting in an upper bound for the maximum separation. Meanwhile, we can find a lower bound on the maximum intersatellite separation by considering the use of slow detectors. A slow detector at the receiver will not be able to resolve pointing errors, resulting in a lossy channel with fixed transmissivity averaged over the entire fading process. Interestingly, the rate in bits per channel use via slow detection can in some instances be higher than that for fast detectors, which resolve the fading dynamics. However, the slower detection time severely limits the operational rate at which the channel can be used (or clock rate). As a result, the point-to-point communication rate via slow detection will be orders of magnitude smaller than those with fading-resolving setups. This information can be used to write a lower bound on  $z_b^{\max}$ . For explicit details on these bounds, see the Supplemental Material [51].

The maximum intersatellite separation  $z_b^{\max}$  describes a maximum tolerable channel length permitted within the

TABLE I. Parameter table for the fiber and satellite modular network configuration. Here we consider two similar setups using a collimated Gaussian beam at 800-nm wavelength, but differ in initial spot size  $w_0$ , receiver aperture  $a_R$ , and frequency filter  $\Delta\lambda$ .

Parameter	Symbol	Value
Beam curvature	$R_0$	$\infty$
Wavelength	$\lambda$	800 nm
Initial spot size	$w_0$	40 cm setup (1)
		20 cm setup (2)
Receiver aperture	$a_R$	1 m setup (1)
		40 cm setup (2)
Detector efficiency	$\eta_{\text{eff}}$	0.4
Detector noise	$\bar{n}_{\text{ex}}$	$\approx 0$
Pointing error	$\sigma_p^2$	$1 \mu\text{rad} \approx (10^{-6}z)^2$
Pulse duration	$\Delta t$	10 ns
Field of view	$\Omega_{\text{FOV}}$	$10^{-10}$ sr
Frequency filter	$\Delta\lambda$	0.1 pm setup (1)
		1 nm setup (2)
Intercommunity link	ICL	Downlink
Fiber loss rate	$\gamma$	0.02 per km

backbone network. Yet, it is not always true that such a channel length is achievable due to line-of-sight limitations associated with orbital geometry. This is quantified by the maximum line-of-sight distance from Eq. (44), a function of the altitudes of the communicating satellites. Crucially, if we find that  $z_b^{\text{max}} \geq z_{\text{sight}}^{\text{max}}$  for some network configuration and desirable rate, this means that the satellites within the backbone can reliably communicate with *any* other satellite that fall within its line of sight, without compromising performance. This is an extremely useful property, providing significant flexibility for satellite backbone networks.

### 3. Discussion

Figure 4 offers insight into the constraints proposed by Corollary 2 for satellite-fiber modular networks corresponding to a number of different physical settings and network properties. Here we consider two free-space communication setups described in Table I: setup (1) in (a) and (c) and setup (2) in (b) and (d).

Consider a flooding capacity  $\mathcal{C}^m(\mathcal{N})$  that is desired between the two end users who are located in remote, fiber communities. The actual ground distance between the users or unique communities is irrelevant, and can be arbitrarily situated at any location across the Earth. If that flooding capacity is to be achieved, then for a given modular architecture there exists a maximum fiber length  $d_{c_j}^{\text{max}}$  permitted within the user community  $c_j$ , and a maximum intersatellite separation  $z_b^{\text{max}}$  permitted throughout the backbone network.

In Figs. 4(a) and 4(b) we plot the behavior of the maximum intersatellite separation with respect to desired

flooding capacity. In the solid lines, we plot the worst case  $z_b^{\text{max}}$ , which corresponds to the situation where all the downlink channels are connected to the same node on the backbone, allocating a single satellite to connect to a community. This is a worst-case situation because it means that the minimum cut on the backbone is very small,  $H_{\text{min}}^* = k_b$ . Yet, even in this scenario, thanks to the lack of atmospheric decoherence we find that very large distances are permitted between satellites, such that  $z_b^{\text{max}} \sim 10^3 - 10^4$  km can still ensure high flooding rates between the end-user communities on the Earth.

Meanwhile, the dashed lines plot  $z_b^{\text{max}}$  for the best-case spatial distribution of downlink connections on the backbone when the maximum satellite altitude is  $h^{\text{max}} = 1500$  km and all downlink beam trajectories are within a 1 steradian angular window. This means that the smallest backbone cut set has the total number of edges

$$H_{\text{min}}^* = k_b |P_{b|c_j}|. \quad (66)$$

In this case, the minimum cut-set cardinality on the backbone is very large, as the number of downlink channels must be increased in order to obtain the chosen flooding capacity. In this best-case scenario, as  $\mathcal{C}^m(\mathcal{N})$  increases  $z_b^{\text{max}}$  begins to plateau, permitting large intersatellite separations even at large flooding capacities. This confirms a strong dependence between the distribution of intercommunity edges and the single-edge capacity properties of a backbone network. For all other distributions of intercommunity connections  $P_{b|c_j}$ , the behavior of the maximum intersatellite separation falls between these bounds.

We also display the maximum line-of-sight distance  $z_{\text{sight}}^{\text{max}} \approx 5428$  km between any pair of satellites orbiting at an altitude  $h^{\text{max}} = 1500$  km. This is the longest intersatellite channel that can be established due to orbital geometry. Interestingly, even in the worst-case backbone configuration (each community possesses many connections to a single satellite) the line-of-sight limit is exceeded by  $z_b^{\text{max}}$  at relatively good rates such that  $\mathcal{C}^m(\mathcal{N}) \in [10^{-2}, 10^{-1}]$  bits per network use. When  $z_b^{\text{max}} \geq z_{\text{sight}}^{\text{max}}$  is true, satellites in the backbone may connect to any other satellite within its line of sight; hence this promises achievable and flexible constraints for intersatellite networks.

Figures 4(c) and 4(d) depict the maximum fiber lengths permitted within  $k_{c_j}$ -connected community networks to ensure a desired end-to-end flooding capacity. Of course, the quality of the bosonic lossy channels do not change with respect to setups (1) and (2) and therefore (c) and (d) are identical. As one would expect, the permissible channel lengths for strong end-to-end rates depend upon the community channels being  $d_{c_j}^{\text{max}} \lesssim 100$  km, even in a highly connected network setting. But thanks to the modular network configuration, this is not problematic. In this configuration, the community fiber networks are designed to cover small areas (relative to the satellite backbone) and

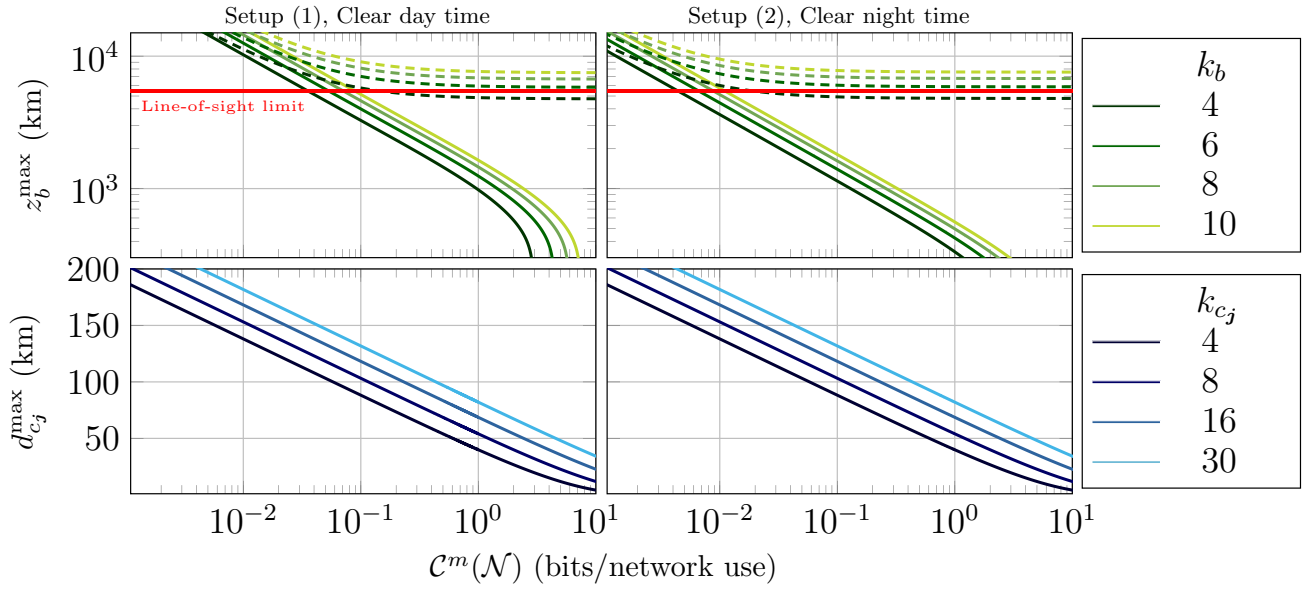


FIG. 4. Optimal end-to-end performance for an ideal modular network consisting of fiber communities interconnected to a satellite-based backbone. In order to guarantee an optimal flooding rate along the  $x$  axis then the maximum internodal separations in each subnetwork on the  $y$  axis must be less than or equal to the plotted bounds. We consider operational settings in setup (1) for (a),(c) and setup (2) for (b),(d), which are described in Table I. The weather and time conditions are those experienced by the worst-case end-user community. Given an optimal flooding capacity  $\mathcal{C}^m(\mathcal{N})$ , we plot the maximum intersatellite separation  $z_b^{\max}$  for different backbone connectivity parameters, and the maximum fiber length in each community  $d_{c_j}^{\max}$  for different community connectivity parameters. The dashed lines in (a) and (c) plot an upper bound of the maximum intersatellite separation based on the optimal spatial distribution of (a finite number of) community-connected satellite nodes  $P_{b|c_j}$  at a maximum altitude  $h^{\max} = 1500$  km, while the solid lines plot the lower bound based on the worst spatial distribution (for any altitude). The red line indicates the maximum achievable channel length that can be achieved for two satellites at altitude 1500 km, such that  $z_{\text{sight}}^{\max} \approx 5428$  km.

facilitate local communication. Quantum communication over global distances is then appropriately mediated by the satellite backbone.

As an example, let us focus on setup (1) and consider a satellite backbone network with regularity  $k_b = 4$  used to mediate long-distance quantum communication between two end users  $\{\alpha, \beta\}$  contained within fiber networks, which are  $k_{c_\alpha} = 4$  and  $k_{c_\beta} = 8$  connected. What are the network constraints required to ensure that their flooding capacity is  $\mathcal{C}^m(\mathcal{N}) = 1$  bit per network use? Provided that  $z_b^{\max} \lesssim 1000$  km, that  $d_{c_\alpha}^{\max} \lesssim 30$  km and  $d_{c_\beta}^{\max} \lesssim 50$  km, then it is guaranteed that this flooding rate is achievable. This provides extremely valuable information for future quantum network designs; if an ideal modular network cannot exceed these constraints, then less ideal structures should take even stronger heed of them.

## B. Ground-based free-space and fiber configuration

### 1. Motivation

It is also interesting to investigate the limits of ground-based quantum networks, which are composed from a mixture of fiber channels and free-space channels. For this purpose, modular network architectures offer an appropriate and physically relevant model. One may consider a

metropolitan network area, which is spanned by a collection of free-space quantum networks, or “hotspots.” These are short-range communities within which reliable free-space quantum communications can take place. In order to communicate over a larger area and between free-space communities we can use an underlying optical-fiber backbone, which mediates longer distance communication.

Utilizing the recently derived ultimate limits of ground-based, free-space quantum communication [32] we wish to determine whether free-space links are reliable enough to enable high-rate quantum communication in this setting. Furthermore, it is important to understand the requirements of the optical-fiber backbone required to facilitate wireless quantum networking.

### 2. Optimal performance

It is possible to once more translate Theorem 1 to establish conditions for which the flooding capacity is given by the global-community capacity, ensuring optimal end-to-end performance. Now, each community is a ground-based free-space community located at an altitude of  $h = 30$  m, and we consider the intercommunity edges connecting each community to the backbone to also be free-space

links. Furthermore, since our rigorous free-space capacities are restricted to the regime of weak turbulence, then we must investigate free-space channels  $\mathcal{E}_{xy}$ , which are no longer than  $z_{xy} \approx 1066$  m [32].

While this may at first appear restrictive, we remind the reader of the physical context; free-space communities are inherently designed for short-range networks with mobile users. Indeed, with network nodes that are limited to line-of-sight connections in a potentially urban area, focusing on the weakly turbulent range is natural. This leaves us with the remaining questions: are free-space quantum channels resilient enough within this range to offer high-rate communication, and what are the resource requirements of the fiber backbone? We provide insight in the following corollary.

**Corollary 3.** *Consider an ideal modular network of the form  $\mathcal{N}^*$  introduced in Definition 3, and assume free-space community networks  $\mathcal{N}_{c_\alpha}$ ,  $\mathcal{N}_{c_\beta}$  and an optical-fiber backbone  $\mathcal{N}_b$ . Select any pair of end users  $\{\alpha, \beta\}$  located in unique communities  $\alpha \in P_{c_\alpha}$  and  $\beta \in P_{c_\beta}$ . There exists a maximum free-space link length in each community*

$$z_{c_j}^{\max} \leq \arg \min_z \left| \log \left( \frac{k_{c_j} \mathcal{L}_{F_\sigma}(\eta, \bar{n}_j)}{\mathcal{C}_{c:b}^m} \right) \right|, \quad (67)$$

and a maximum fiber length in the backbone

$$d_b^{\max} := -\frac{1}{\gamma} \log_{10} \left( 1 - 2^{-\mathcal{C}_{c:b}^m / H_{\min}^*} \right), \quad (68)$$

for which the network flooding capacity is equal to the global-community capacity,

$$\mathcal{C}^m(\mathcal{N}) = \mathcal{C}_{c:b}^m. \quad (69)$$

Otherwise, if any fiber links violate this condition  $\exists d_{xy} > d_b^{\max}$ ,  $(\mathbf{x}, \mathbf{y}) \in E_b$  or the local community links are in violation,  $\exists z_{xy} > z_{c_j}^{\max}$ ,  $(\mathbf{x}, \mathbf{y}) \in E_{c_j}$ , for either  $\mathbf{j} \in \{\alpha, \beta\}$ , then this becomes an upper bound on the network flooding capacity,  $\mathcal{C}^m(\mathcal{N}) \leq \mathcal{C}_{c:b}^m$ .

Notice that we now obtain an upper bound on the maximum free-space link length, as it is not known whether the single-edge quantity  $\mathcal{L}_{F_\sigma}(\eta, \bar{n}_j)$  is achievable or not. However, this bound has been shown to be tight and thus offers an accurate bound on  $z_{c_j}^{\max}$  [32]. Furthermore, this maximum free-space link length must be computed numerically due to the complex nature of the free-space PLOB bound, which accounts for fading and thermal effects. Yet, the maximum fiber length within the backbone can be readily determined for an arbitrary distribution of intercommunity connections.

### 3. Discussion

Figure 5 provides example network constraints using Corollary 3 for ideal modular networks and a variety of community and backbone connectivity properties. Operational parameters are found in Table II for this modular architecture. Given a desired end-to-end flooding capacity, we generate a maximum fiber length in the backbone  $d_b^{\max}$  and maximum free-space link length in each community  $z_{c_j}^{\max}$  in Figs. (a) and (b), respectively, such that this flooding capacity is achieved by the global-community capacity.

Immediately we notice that the flooding capacities plotted are large. This is because, as seen in Fig. 5(b), the free-space links are sufficiently capable in the weakly turbulent regime so that  $z_{c_j}^{\max} > 1$  km for flooding capacities as high as  $\mathcal{C}^m(\mathcal{N}) \approx 2$  bits/network use, even when the community connectivity is low, e.g.,  $k_{c_j} = 4$ . As the community connectivity gets larger, the free-space capacities become increasingly reliable within this distance range, and do not compromise the minimum cut until the flooding capacity becomes very large.

Yet, these large end-to-end capacities simultaneously place greater demands on the backbone network, demanding shorter links as the global-community capacity increases. The solid lines in Fig. 5(b) plot the maximum fiber length corresponding to the worst-case spatial distribution of free-space connections from the communities to the backbone, i.e., all intercommunity links are focussed on a single backbone node. Meanwhile, the dashed lines consider a best-case scenario in which all the intercommunity links are of maximum length  $z_{c:b} = 1$  km, and are oriented such that they maximize the backbone cut-set cardinality  $H_{\min}^* = k_b |P_{b|c_j}|$ .

We find that this free-space and fiber modular architecture reports very feasible constraints on the free-space

TABLE II. Parameter table for the free-space and fiber modular network configuration.

Parameter	Symbol	Value
Beam curvature	$R_0$	$\infty$
Wavelength	$\lambda$	800 nm
Initial spot size	$\omega_0$	5 cm
Receiver aperture	$a_R$	5 cm
Detector efficiency	$\eta_{\text{eff}}$	0.5
Detector noise	$\bar{n}_{\text{ex}}$	0.05
Pointing error	$\sigma_p^2$	$1 \mu\text{rad} \approx (10^{-6}z)^2$
Pulse duration	$\Delta t$	10 ns
Field of view	$\Omega_{\text{FOV}}$	$10^{-10}$ sr
Frequency filter	$\Delta \lambda$	1 nm
Altitude	$h$	30 m
Fiber loss rate	$\gamma$	0.02 per km
Intercommunity link	ICL	Free space (Clear day time)

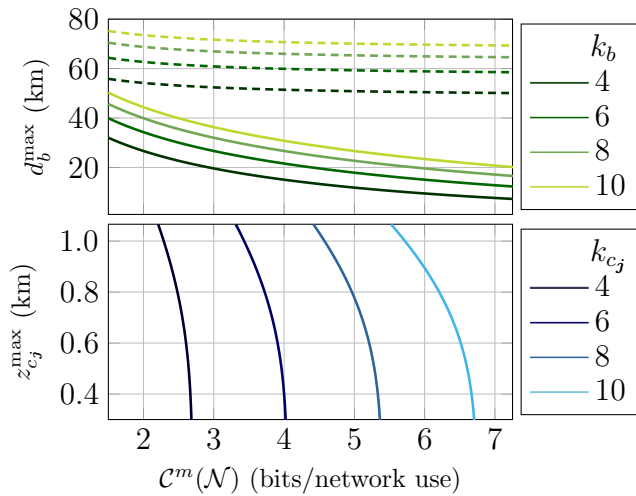


FIG. 5. Optimal end-to-end performance for an ideal modular network consisting of free-space communities interconnected to a fiber-based backbone. In order to guarantee an optimal flooding rate along the  $x$  axis then the maximum internodal separations in each subnetwork depicted on the  $y$  axis must be less than or equal to the plotted bounds. We use the operational settings in Table II during clear day time. Given an optimal flooding capacity  $\mathcal{C}^m(\mathcal{N})$ , we plot the maximum fiber length  $d_b^{\max}$  for different backbone connectivity parameters, and the maximum free-space link length in each community  $z_{c_j}^{\max}$  for different community connectivity parameters. The dashed lines plot an upper bound on the maximum fiber length based on the optimal spatial distribution of community-connected backbone nodes  $P_{b|c_j}$ , while the solid lines plot a lower bound based on the worst-case spatial distribution.

hotspots and fiber backbone in order to guarantee a high end-to-end performance. For a regular fiber-based backbone with  $k_b = 4$ , and end-user communities, which are  $k_{c_j} > 4$  connected, then one can guarantee an achievable flooding capacity of  $\mathcal{C}^m(\mathcal{N}) = 2$  bits/network use given that the free-space links all fall within the weakly turbulent range, and at worst  $d_b^{\max} \lesssim 25$  km. Within a metropolitan setting, such constraints can be satisfied with realistic resources, supporting the development of wireless quantum networks. Furthermore, confidence in the use of free-space links within this setting reduces the need for wired fiber connections in small areas.

## V. CONCLUSION

In this work we investigate the end-to-end capacities of free-space and hybrid quantum networks, combining recently developed results in quantum-information theory and well-established theories of free-space optical communication. After collecting and reviewing these recent results, we introduce a modular network architecture for the purposes of constructing hybrid quantum networks using both free-space and fiber links. With these tools in hand, we specify our analysis to ideal modular networks,

which utilize an underlying regular backbone. Through this ideality it is possible to study ultimate limits for highly relevant modular architectures, revealing critical network properties that assure optimal performance.

We perform a detailed analysis of the ultimate limits of a satellite-based quantum internet; leveraging the properties of fiber networks on the ground, ground-satellite connective structures and intersatellite networks in space. This theoretically demonstrates that high-rate global quantum communication can be efficiently mediated by a satellite quantum network with realistic connectivities and tolerable intersatellite separations on the order of approximately  $10^3 - 10^4$  km. Such designs allow for effective quantum communication between arbitrarily distant end users on the Earth. These analyses also indicate that careful consideration of the spatial distribution of ground-satellite connections can more effectively alleviate separation constraints, rather than increasing the nodal degree.

Furthermore, we study the ultimate limits of a free-space and fiber modular network configuration, discussing the efficacy of free-space subnetworks within metropolitan areas. We show that within the weakly turbulent regime (where free-space links are limited to approximately 1 km) high-rate intercommunity communication can be readily achieved, using a fiber backbone with realistic resources.

These results offer promising steps in the direction of understanding the ultimate limits of free-space and hybrid quantum networks; motivating its future study both theoretically and experimentally. Our analyses offer a rigorous demonstration of the efficacy of free-space quantum links in a network setting, emphasizing that the integration of free-space and fiber can be reliably performed within future quantum networks. Hybrid architectures can and should be designed to take advantage of the strengths of different modes of quantum communication. This work may serve as a platform for future investigations that account for full technical details of the nodes; exploiting these tools to study more realistic, random architectures of hybrid networks, which can be benchmarked against the ideal designs studied here.

## ACKNOWLEDGMENTS

C.H and A.I.F acknowledge funding from the EPSRC via a Doctoral Training Partnership (EP/R513386/1). S.P. acknowledges funding by the European Union via ‘‘Continuous Variable Quantum Communications’’ (CiViQ, Grant Agreement No. 820466).

- 
- [1] P. Slepian, *Mathematical Foundations of Network Analysis* (Springer-Verlag, New York, 1968).
  - [2] T. M. Cover and J. A. Thomas, *Elements of Information Theory* (Wiley, New Jersey, 2006).

- [3] A. S. Tanenbaum and D. J. Wetherall, *Computer Networks* (Pearson, 2010), 5th ed.
- [4] A. El Gamal and Y.-H. Kim, *Network Information Theory* (Cambridge University Press, Cambridge, 2011).
- [5] H. J. Kimble, The quantum internet, *Nature* **453**, 1023 (2008).
- [6] S. Pirandola and S. L. Braunstein, Physics: Unite to build a quantum internet, *Nature* **532**, 169 (2016).
- [7] M. Razavi, *An Introduction to Quantum Communications Networks* (Morgan & Claypool Publishers, 2018), p. 2053.
- [8] S. Pirandola, U. L. Andersen, L. Banchi, M. Berta, D. Bunandar, R. Colbeck, D. Englund, T. Gehring, C. Lupo, and C. Ottaviani, *et al.*, Advances in quantum cryptography, *Adv. Opt. Photonics* **12**, 1012 (2020).
- [9] S. Pirandola, R. García-Patrón, S. L. Braunstein, and S. Lloyd, Direct and Reverse Secret-Key Capacities of a Quantum Channel, *Phys. Rev. Lett.* **102**, 050503 (2009).
- [10] S. Pirandola, R. Laurenza, C. Ottaviani, and L. Banchi, Fundamental limits of repeaterless quantum communications, *Nat. Commun.* **8**, 15043 (2017).
- [11] S. Pirandola, End-to-end capacities of a quantum communication network, *Commun. Phys.* **2**, 51 (2019).
- [12] Q. Zhuang and B. Zhang, Quantum communication capacity transition of complex quantum networks, *Phys. Rev. A* **104**, 022608 (2021).
- [13] B. Zhang and Q. Zhuang, Quantum internet under random breakdowns and intentional attacks, *Quantum Sci. Technol.* **6**, 045007 (2021).
- [14] C. Harney and S. Pirandola, Analytical Methods for High-Rate Global Quantum Networks, *PRX Quantum* **3**, 10349 (2022).
- [15] S.-K. Liao, J. Lin, J. Ren, W. Liu, J. Qiang, J. Yin, Y. Li, Q. Shen, L. Zhang, and Y. Cao, *et al.*, Space-to-Ground Quantum Key Distribution Using a Small-Sized Payload on Tiangong-2 Space Lab, *Chin. Phys. Lett.* **34**, 090302 (2017).
- [16] J. Yin, Y. Cao, Y.-H. Li, S.-K. Liao, L. Zhang, J.-G. Ren, W.-Q. Cai, W.-Y. Liu, B. Li, H. Dai, and G.-B. Li, *et al.*, Satellite-based entanglement distribution over 1200 kilometers, *Science* **356**, 1140 (2017).
- [17] J.-G. Ren, P. Xu, H.-L. Yong, L. Zhang, S.-K. Liao, J. Yin, W.-Y. Liu, W.-Q. Cai, M. Yang, and L. Li, *et al.*, Ground-to-satellite quantum teleportation, *Nature* **549**, 70 (2017).
- [18] J. Yin, Y.-H. Li, S.-K. Liao, M. Yang, Y. Cao, L. Zhang, J.-G. Ren, W.-Q. Cai, W.-Y. Liu, S.-L. Li, and R. Shu, *et al.*, Entanglement-based secure quantum cryptography over 1,120 kilometres, *Nature* **582**, 501 (2020).
- [19] A. Villar, A. Lohrmann, X. Bai, T. Vergoossen, R. Bedington, C. Perumangatt, H. Lim, T. Islam, A. Reezwana, and Z. Tang, *et al.*, Entanglement demonstration on board a nano-satellite, *Optica* **7**, 734 (2020).
- [20] Y.-A. Chen, Q. Zhang, T.-Y. Chen, W.-Q. Cai, S.-K. Liao, J. Zhang, K. Chen, J. Yin, J.-G. Ren, Z. Chen, and S.-L. Han, *et al.*, An integrated space-to-ground quantum communication network over 4,600 kilometres, *Nature* **589**, 214 (2021).
- [21] J. S. Sidhu, S. K. Joshi, M. Gündoğan, T. Brougham, D. Lowndes, L. Mazzarella, M. Krutzik, S. Mohapatra, D. Dequal, and G. Vallone, *et al.*, Advances in space quantum communications, *IET Quant. Comm.* **2**, 182 (2021).
- [22] M. A. Nielsen and I. L. Chuang, *Quantum Computation and Quantum Information: 10th Anniversary Edition* (Cambridge University Press, USA, 2011), 10th ed.
- [23] C. Weedbrook, S. Pirandola, R. García-Patrón, N. J. Cerf, T. C. Ralph, J. H. Shapiro, and S. Lloyd, Gaussian quantum information, *Rev. Mod. Phys.* **84**, 621 (2012).
- [24] A. Serafini, *Quantum Continuous Variables: A Primer of Theoretical Methods* (CRC Press, Taylor & Francis Group, Boca Raton, FL, 2017).
- [25] J. Goodman, *Statistical Optics* (John Wiley & Sons, New York, 1985).
- [26] O. Svelto, *Principles of Lasers* (Springer, New York, 2010), 5th ed.
- [27] C. Bohren and D. Huffman, *Absorption and Scattering of Light by Small Particles* (John Wiley & Sons, New York, 1983).
- [28] V. Tatarskii, *The Effects of the Turbulent Atmosphere on Wave Propagation* (Israel Program for Scientific Translations, Jerusalem, 1971).
- [29] A. Majumdar and J. Ricklin, *Free-Space Laser Communications* (Springer, New York, 2008).
- [30] H. Kaushal, V. Jain, and S. Kar, *Free Space Optical Communication* (Springer, New York, 2017).
- [31] L. Andrews and R. Phillips, *Laser Beam Propagation Through Random Medium* (SPIE, Bellingham, 2005).
- [32] S. Pirandola, Limits and security of free-space quantum communications, *Phys. Rev. Res.* **3**, 013279 (2021).
- [33] S. Pirandola, Satellite quantum communications: Fundamental bounds and practical security, *Phys. Rev. Res.* **3**, 023130 (2021).
- [34] J. Borregaard, H. Pichler, T. Schröder, M. D. Lukin, P. Lodahl, and A. S. Sørensen, One-Way Quantum Repeater Based on Near-Deterministic Photon-Emitter Interfaces, *Phys. Rev. X* **10**, 021071 (2020).
- [35] L. Childress, J. M. Taylor, A. S. Sørensen, and M. D. Lukin, Fault-Tolerant Quantum Communication Based on Solid-State Photon Emitters, *Phys. Rev. Lett.* **96**, 070504 (2006).
- [36] C. Simon, H. de Riedmatten, M. Afzelius, N. Sangouard, H. Zbinden, and N. Gisin, Quantum Repeaters with Photon Pair Sources and Multimode Memories, *Phys. Rev. Lett.* **98**, 190503 (2007).
- [37] V. C. Usenko, B. Heim, C. Peuntinger, C. Wittmann, C. Marquardt, G. Leuchs, and R. Filip, Entanglement of gaussian states and the applicability to quantum key distribution over fading channels, *New J. Phys.* **14**, 093048 (2012).
- [38] P. Papanastasiou, C. Weedbrook, and S. Pirandola, Continuous-variable quantum key distribution in uniform fast-fading channels, *Phys. Rev. A* **97**, 032311 (2018).
- [39] S. Pirandola, R. Laurenza, and L. Banchi, Conditional channel simulation, *Ann. Phys. (N. Y.)* **400**, 289 (2019).
- [40] The word *tight* in this context refers to how close the upper bound is from its best known lower bound. Indeed, there exists a lower bound on the capacity of a point-to-point thermal-loss channel based on its reverse coherent information (RCI) [53]. Hence, throughout our work we implicitly refer to tight upper bounds on thermal-loss channel capacities (and subsequently, network capacities) as those, which in conjunction with the RCI, can tightly sandwich the exact capacity.

- [41] D. Medhi and K. Ramasamy, *Network Routing: Algorithms, Protocols, and Architectures* (Morgan Kaufmann publishers, Cambridge MA, 2018), 2nd ed.
- [42] N. R. Solomons, A. I. Fletcher, D. Aktas, N. Venkatachalam, S. Wengerowsky, M. Lončarić, S. P. Neumann, B. Liu, Željko Samec, M. Stipčević, and R. Ursin, *et al.*, Scalable Authentication and Optimal Flooding in a Quantum Network, *PRX Quantum* **3**, 020311 (2022).
- [43] L. R. Ford and D. R. Fulkerson, Maximal flow through a network, *Can. J. Math.* **8**, 399 (1956).
- [44] J. Edmonds and R. M. Karp, Theoretical improvements in algorithmic efficiency for network flow problems, *J. ACM* **19**, 248 (1972).
- [45] J. B. Orlin, in *Proceedings of the forty-fifth annual ACM symposium on Theory of computing, STOC'13* (2013), p. 765.
- [46] M. Ghalaii and S. Pirandola, Quantum communications in a moderate-to-strong turbulent space, (2021), [ArXiv:arXiv:2107.12415](https://arxiv.org/abs/2107.12415).
- [47] R. Fante, Electromagnetic beam propagation in turbulent media, *Proc. IEEE* **63**, 1669 (1975).
- [48] R. Fante, Electromagnetic beam propagation in turbulent media: An update, *Proc. IEEE* **68**, 1424 (1980).
- [49] H. T. Yura, Short-term average optical-beam spread in a turbulent medium, *J. Opt. Soc. Am.* **63**, 567 (1973).
- [50] B. Gross, D. Vaknin, S. V. Buldyrev, and S. Havlin, Two transitions in spatial modular networks, *New J. Phys.* **22**, 053002 (2020).
- [51] See the Supplementary Material <http://link.aps.org/supplemental/10.1103/PhysRevApplied.18.014012> for definitions, lemmas, theorems, and their proofs for theoretical developments discussed in the main text. This includes discussions of networks with community structures from which this modular network emerges as a useful and highly desirable class.
- [52] While it might be more convenient to call this the *intercommunity capacity*, such a name might be confused as a more general term for the capacity when the end users are located in different communities (which is implied). The global-community capacity is intended to be more distinct than this, and specify a particular network cut.
- [53] R. García-Patrón, S. Pirandola, S. Lloyd, and J. H. Shapiro, Reverse Coherent Information, *Phys. Rev. Lett.* **102**, 210501 (2009).